Genetic mechanisms underlying East Asian and European Facial differentiation

Sijia Wang (wangsijia@picb.ac.cn)
CAS Key Laboratory of Computational Biology, Shanghai Institutes of Nutrition and Health, University of Chinese Academy of Sciences, Chinese Academy of Sciences https://orcid.org/0000-0001-6961-7867

Manfei Zhang
MOE Key Laboratory of Contemporary Anthropology, School of Life Sciences, Fudan University
https://orcid.org/0000-0003-2611-9440

Sijie Wu
State Key Laboratory of Genetic Engineering and Ministry of Education Key Laboratory of Contemporary Anthropology, Collaborative Innovation Center for Genetics and Development, School of Life Scienc

Siyuan Du
CAS Key Laboratory of Computational Biology, Shanghai Institute of Nutrition and Health, University of Chinese Academy of Sciences, Chinese Academy of Sciences https://orcid.org/0000-0003-1602-1669

Wei Qian
Human Phenome Institute, Fudan University

Jieyi Chen
State Key Laboratory of Genetic Engineering and Ministry of Education Key Laboratory of Contemporary Anthropology, Collaborative Innovation Center for Genetics and Development, School of Life Scienc

Lu Qiao
CAS Key Laboratory of Computational Biology, Shanghai Institute of Nutrition and Health, University of Chinese Academy of Sciences, Chinese Academy of Sciences

Yajun Yang
Fudan University

Jingze Tan
Fudan University

Nicolas Navarro
Biogéosciences, UMR 6282 CNRS, EPHE, Université Bourgogne Franche-Comté, Dijon 21078, France.
https://orcid.org/0000-0001-5694-4201

Kun Tang
CAS Key Laboratory of Computational Biology, Shanghai Institute of Nutrition and Health, University of Chinese Academy of Sciences, Chinese Academy of Sciences

Andres Ruiz-Linares
Fudan University https://orcid.org/0000-0001-8372-1011

Peter Claes

University of Leuven https://orcid.org/0000-0001-9489-9819

Li Jin

Fudan Univesity

Jiarui Li

CAS Key Laboratory of Computational Biology, Shanghai Institute of Nutrition and Health, University of Chinese Academy of Sciences, Chinese Academy of Sciences https://orcid.org/0000-0003-0581-5850

Article

Keywords: facial morphology, East Asian and European Facial differentiation, genetic mechanisms

Posted Date: June 23rd, 2021

DOI: https://doi.org/10.21203/rs.3.rs-604881/v1

Genetic mechanisms underlying East Asian and European Facial differentiation

Manfei Zhang[1,2,3,14], Sijie Wu[1,2,4,14], Siyuan Du[2,14], Wei Qian[1,2,3,14], Jieyi Chen[2,4], Lu Qiao[2], Yajun Yang[4], Jingze Tan[4], Nicolas Navarro[5,6], Kun Tang[2], Andrés Ruiz-Linares[1,4,7,8], Peter Claes[9,10,11,12], Li Jin[1,2,4,*], Jiarui Li[2,9,10,*] & Sijia Wang[1,2,13,*]

[1] Human Phenome Institute, Fudan University, 825 Zhangheng Road, Shanghai, China.

[2] CAS Key Laboratory of Computational Biology, Shanghai Institute of Nutrition and Health, University of Chinese Academy of Sciences, Chinese Academy of Sciences, 320 Yue Yang Road, Shanghai 200031, China.

[3] School of Computer Science, Fudan University, 2005 Songhu Road, Shanghai, China

[4] State Key Laboratory of Genetic Engineering and Ministry of Education Key Laboratory of Contemporary Anthropology, Collaborative Innovation Center for Genetics and Development, School of Life Sciences, Fudan University, Shanghai, China.

[5] Biogéosciences, UMR 6282 CNRS, EPHE, Université Bourgogne Franche-Comté, Dijon 21078, France.

[6] EPHE, PSL University, Paris 75014, France.

[7] Aix-Marseille Université, CNRS, EFS, ADES, Marseille, 13005, France.

[8] Department of Genetics, Evolution and Environment, and UCL Genetics Institute, University College London, London WC1E 6BT, UK.

[9] Department of Electrical Engineering, ESAT/PSI, KU Leuven, Leuven, Belgium

[10] Medical Imaging Research Center, UZ Leuven, Leuven, Belgium.

[11] Department of Human Genetics, KU Leuven, Leuven, Belgium.

[12] Murdoch Children's Research Institute, Melbourne, Victoria, Australia.

[13] Center for Excellence in Animal Evolution and Genetics, Chinese Academy of Sciences, Kunming 650223 China.

[14] These authors contributed equally: Manfei Zhang, Sijie Wu, Siyuan Du, Wei Qian.

[*] Corresponding authors.

Abstract

Facial morphology, the most conspicuous feature of human appearance, is highly heritable. Previous studies on the genetic basis of facial morphology were mainly performed in European populations. Applying a proven data-driven phenotyping and multivariate genome-wide scanning protocol to the largest collection of 3D facial images of an East Asian population to date, we identified 244 leading variants associated with normal-range facial variation, of which 130 are novel. A newly proposed polygenic shape analysis indicates that the effects of the variants on East Asian facial shape can be generalized into the European population. Based on this analysis, we further identified 13 variants mainly related to differences between European and East Asian facial shape. Natural selection analyses suggest that the difference in European and East Asian nose shape is caused by a directional selection, mainly due to a local adaptation in Europeans. Our results expand the knowledge of human facial genetics and illustrates for the first time the underlying genetic basis for facial differences across populations.

Main Text

Facial morphology, the most conspicuous feature of human appearance, has substantial variations at the individual and population level. Multiple studies show significant differences across different geographic regions of people in craniofacial morphology[1-18]. For example, Europeans have a more protruding nose and brow ridges than East Asians[19]. Such differences must have a strong genetic basis, which remains unknown, mainly due to the unbalanced amount of research in European versus non-European populations. Previous genetic studies combined report about 300 signals associated with facial morphology in European populations, but only 22 are reported in East Asians or Eurasians, about 21 in Latin American and 10 in African[2,3,5-7,10,14-16]. Large-scale studies in East Asians and other non-European populations are much needed to provide a complete architecture of the genetic basis of facial morphology, particularly the observable differences across populations.

Here we performed a genome-wide association study (GWAS) based on the largest collection of 3D facial images in Han Chinese populations to date. Using a proven data-driven phenotyping approach, we successfully identified hundreds of associated variants[1,9]. In addition, we identified specific variants distinguishing between European and East Asian facial appearance. We further provided evidence that those population-based facial differences, especially for nose shape, are under selection. A schematic overview of our study design can be found in Extended Data Figure 1.

GWAS on hierarchical facial phenotypes discovered 244 signals

To study facial variation from a global to local scale, we used 3D facial surface scans from a large-scale East-Asian population (Methods, Supplementary Table 1) in a discovery (n = 6,968) and replication cohort (n = 2,706), and subsequently combined

them in a meta-analysis. A semi-supervised phenotyping procedure defined 63 hierarchically arranged facial segments using the discovery cohort (Methods). Next, we performed a canonical correlation analysis (CCA) based GWAS on each facial segment's group of principal components (PC), which defined the linear combination of PCs that are most correlated with each variant. In the replication cohort, the associations were tested based on projections onto the CCA directions followed by Pearson's correlation. Subsequently, we identified 50 independent tests using parallel analysis and permutation test (Methods)[1,20,21]. Thus, besides conventional genome-wide threshold ($P = 5\times10^{-8}$), we set the stricter study-wide threshold to $P = 1\times10^{-9}$ ($P = 5\times10^{-8}/50$) after Bonferroni correction. In the discovery datasets, we identified 156 genome-wide significant variants ($P < 5\times10^{-8}$) after condition analysis and peak selection (Methods). In which, 81 variants are study-wide significant ($P < 1\times10^{-9}$). Majority of variants (120 out of 156 genome-wide variants, 76 out of 81 study-wide variants) are replicated at nominal threshold ($P < 0.05$). To increase statistical power, we performed a meta-analysis using Stouffer's method to combine the P-values obtained from the discovery and replication cohort[1,22]. As a result, we identified 244 genome-wide threshold independent variants associated with normal range facial variation (Fig. 1a; Supplementary Table 2). In which, 151 variants are study-wide significant. According to the anatomical structure, we classified the 244 genome-wide significant variants in ten facial regions (Methods), including forehead, glabella, eye, tempora, zygoma, nose, maxillary, upper mouth, lower mouth, and mandible (Fig. 1b; Supplementary Table 3). The nose region has most of the variants (107) out of the ten regions. The number of variants associated with the other nine regions ordered from high to low are: glabella (35), upper mouth (32), eye (29), zygoma (28), maxillary (25), mandible (20), forehead (16), lower mouth (13) and tempora (12).

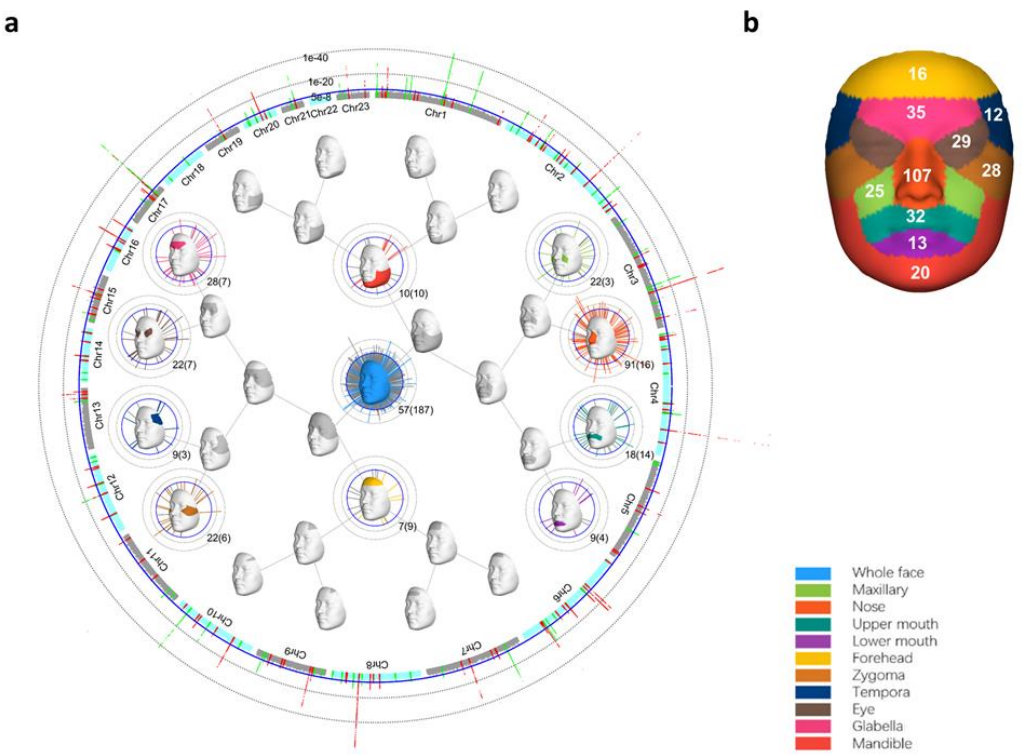

Fig. 1: Overall results of genome-wide association meta-analyses on Han Chinese cohort. a) The Manhattan plot on the ring represents the meta-analyses P-values, with chromosomes colored and labelled. P-values are -log10 scaled. Using 500kb windows, peak variants are colored in red (novel variants) and green (known variants). Inside the Manhattan plot, a binary tree of facial segments illustrates the hierarchical facial segmentation up to level four. On the whole face and ten selected facial segments (colored), variants in the segment itself (colored) and in its children segments (gray) are plotted, with the number of variants listed (#variants in children segments in parenthesis). b) Visualization of ten selected facial segments and number of significant variants.

We considered a variant as novel when it was not in LD ($r^2 < 0.1$) with previously reported variants (P-values in facial GWAS $< 5\times10^{-8}$, Supplementary Table 7) in all of the East Asian (EAS, including CHB, and CHS), European (EUR, including TSI, GBR, IBS, and CEU), or African (YRI) populations in the 1000 Genomes Project phase 3 (1000GP)[23]. As such, 130 of the 244 leading variants below the genome-wide threshold

are novel, while 65 of the 151 leading variants below the study-wide threshold are novel. (Supplementary Table 2).

We used FUMA and GREAT to annotate the leading variants[24,25]. As a result, we identified 204 potential genes associated with facial variation. In which, 100 genes are not reported in previous facial GWAS studies (Supplementary Table 2). Besides, we found that the genes associated with the leading variants are highly enriched for the processes of skeletal system development and morphogenesis related biological processes (Extended Data Fig. 2a). Moreover, from the epigenome and transcriptome datasets from variable tissue or cell types, the leading variants are mainly enriched for enhancers in craniofacial tissues, and candidate genes are significantly highly expressed in mesenchyme compared to in ectoderm at late fetal development (Extended Data Fig. 2b-c)[26-29]. These findings are consistent with expectations and previous studies[1,26,30].

Characteristics of shared and differentiated signals in East Asian (EAS) and European (EUR) studies

By comparing the 244 leading variants identified in our study with the 203 leading variants reported in a recently published European study using similar phenotyping and analysis framework, 89 genetic loci are shared in both studies (8 variants were the same in both studies, while others are in LD ($r^2 > 0.2$) with variants found in the other population)[1]. The remaining 155 variants of the EAS study and 114 variants of the EUR study are differentiated between two cohorts (Fig. 2a; Supplementary Table 4). Therefore, we define three different groups of variants, the group including the 89 shared variants, a group of 155 EAS differentiated variants, and a group of 114 EUR differentiated variants, respectively.

To understand these shared and differentiated variants' characteristics, we examined their allele frequencies in the East Asian and European populations based on the 1000GP[23]. Comparison of trans-population minor allele frequency (MAF) shows that the differentiated groups of variants have higher MAF in their respective population. In contrast, shared variants have no difference of MAF between two populations (Fig. 2b-e). These results suggest that higher MAFs may increase the statistical power to detect these variants associated with facial variation within the respective populations. Moreover, 77.5% (69 out of 89) of the shared variants are below the study-wide threshold. While only 54.2% (84 out of 155) EAS differentiated variants and 55.2% (63 out of 114) EUR differentiated variants are below the study-wide threshold (chisq.test $P_{EAS} = 3.2\times10^{-4}$; $P_{EUR} = 4.8\times10^{-6}$). It is therefore likely that variants identified in one population with a P-value higher than the study-wide threshold need more statistical power to be detected in another population.

To explore potential biological functional differences of the shared and differentiated variants, we used Metascape to compare the differences of enriched terms for the annotated genes of differentiated and shared variants[31]. We found that EAS differentiated, EUR differentiated and shared genes are all associated with top term clusters that were previously reported to be associated with craniofacial variation (Fig. 2f). Moreover, compared with the direct overlap in genes, a considerable number of functional overlaps among the three groups was observed (Fig. 2g). These results indicate that although the genes are different among the three groups, they might be different parts of the same biological processes. We next compared the epigenetic regulation pattern of shared and differentiated variants in various cell-types or tissues. The differentiated and shared variants are both enriched for enhancers in craniofacial

tissues (Fig. 2h), again indicating that the potential functions of differentiated and shared are analogical.

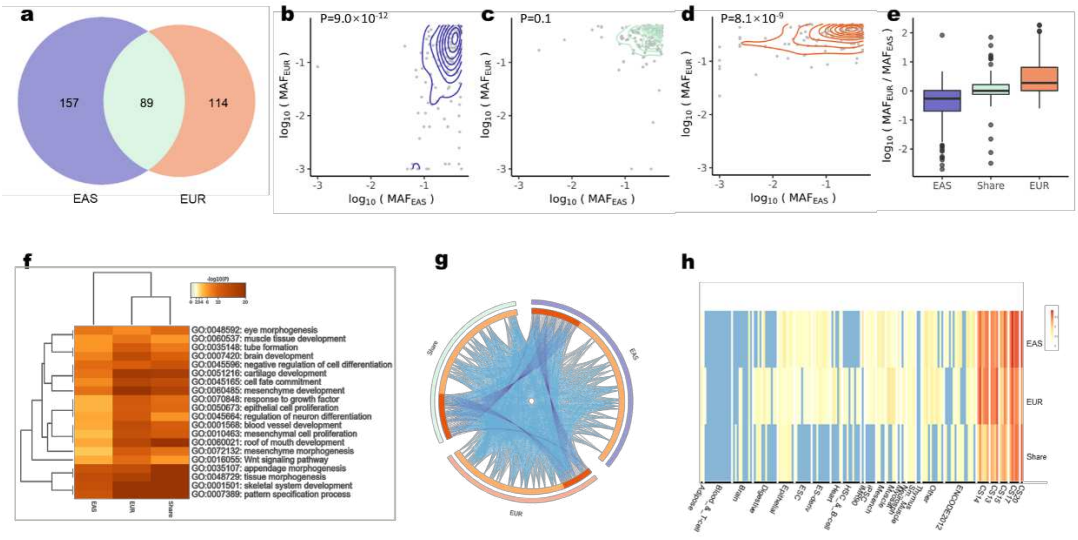

Fig. 2: Comparison of shared and differentiated variants. a) Number differentiated and shared variants of two study cohorts (EAS and EUR). b-e) Trans-ancestral MAF comparisons of b) differentiated variants of EAS (n = 155). c) Shared variants (n = 178 (89 in EAS study and 89 in EUR study), shared variants in both studies are used), and d) differentiated variants of EUR (n = 114). In b-d), P-values are provided using a two-sided Mann-Whitney U-test. When MAF < 0.001, MAF was truncated to 0.001 to fit the log scale (1000GP). e) MAF ratio comparison of three groups. Colors are corresponding with a). f) Metascape analysis shows the biological processes associated with genes in the three groups of genes. g) Each outside arc represents a group, and each inside arc represent a gene list. On the inside, each arc represents a gene list, where each gene has a spot on the arc. The dark orange color represents overlapping genes among groups. Same genes (purple lines) and different genes fell into the same ontology term (blue lines) of three groups. h) Heatmap indicates the global enrichment of trait-associated variants of each group (y axis) in enhancer of different tissue (x axis).

As expected, we found that the differentiated variants have a significantly higher wright's fixation index (F_{ST}) than random variants at a genome-wide scale both in EAS

and EUR populations ($P_{EAS\ differentiated}$ = 2.42×10^{-10}; $P_{EUR\ differentiated}$ = 0.0063, Extended Data Fig 3), while shared variants have no significant difference compared with random variants ($P_{EAS\ shared}$ = 0.599)[32,33]. The same result applies to the Cross Population Extended Haplotype Homozygosity (XP-EHH) analysis using REHH2 in these two populations ($P_{EAS\ differentiated}$ = 0.0078; $P_{EUR\ differentiated}$ = 0.038; $P_{EAS\ shared}$ = 0.449)[34,35]. These results suggest that facial variation in different populations could be attributed to random drift and natural selection. In other words, differentiated variants explained a larger proportion of natural selection between populations, while shared variants may mainly explain random drift influences to facial variation.

In summary, each study's differentiated group of variants is mainly because of a difference in trans-MAF combined with subtle effect sizes. Although they could not be independently discovered in the other population's cohort, the functional enrichment analyses showed that those variants are reliable.

Polygenic shape analysis suggests the generalization of association results from East Asians to Europeans

To explore the genetic basis of what makes an East Asian face and the genetic factors contributing to the difference in facial shape between East Asians and Europeans, we first investigated whether the association results of the leading variants in our study of East Asians could be generalized to Europeans.

We introduced a novel polygenic shape analysis to investigate whether the differentiated accumulated genetic effect between the two populations (caused by allele frequencies differences) of our leading variants is in line with the actual population facial difference. Similar to the classic polygenic score analysis, the Polygenic Shape (PS) for an individual is the sum of the number of effect risk alleles weighted by risk

allele effect size vectors of our leading variants[36]. Similarly, the Polygenic Population Shape (PPS) is the mean polygenic shape for a given population (Methods). Using data of EUR (n = 404, including TSI (107), GBR (91), IBS (107) and CEU (99)) and EAS (n = 208, including CHB (103), and CHS (105)) individuals from 1000GP, we calculated the PPS of the two populations for the whole face and ten anatomical facial regions[23]. Thus, the differentiated accumulated genetic effects on facial shape between the two populations then becomes the difference between two polygenic population shapes; $PPS_{EUR} - PPS_{EAS}$. To visualize and compare this effect to the true population mean facial shapes for each facial region, we constructed EUR and EAS derived shapes by adding and subtracting, respectively, $(PPS_{EUR} - PPS_{EAS})/2$ to and from the overall average facial shape (i.e., a population neutral average face, which was constructed as the average of the EUR and EAS population mean shapes (Methods)).

Firstly, we visualized the EUR and EAS derived faces. We used 3D facial scans of EAS and EUR individuals to calculate each population's average face and therefore generated the EUR and EAS mean faces. Compared with the mean face of EUR, we found that EAS had more protrusion in the cheek; more concavity in the forehead, glabella, nose, and mandible (Fig. 3a-i), which are consistent with a previous study[19]. Interestingly, when we amplify the differentiated accumulated genetic effects five times, the PPS derived faces look remarkably similar to EAS and EUR's actual mean face (Fig. 3a-ii). The EUR and EAS derived whole faces show similar facial variations to the ground truth, especially in the glabella and nose region (Fig. 3a-ii).

To test the generalization of the association results from our study to Europeans, we compared the EUR and EAS derived whole faces using all the 244 leading variants with derived whole faces using 244 randomly chosen genome-wide variants. The EAS and EUR PPS derived faces using the 244 leading variants were significantly more similar

to the true population mean faces than the PPS derived faces using random variants, either measured by Euclidean distance (P = 0.007) or cosine similarity (P_{EUR} = 0.004; P_{EAS} = 0.005; Fig. 3b). Moreover, we calculated individual facial PS for EUR and EAS individuals from 1000GP and measured their East Asian facial similarity (EAS-FS), defined as the projected length of the individual's PS onto the explicit EAS-EUR shape difference (Methods, Supplementary Fig. 2). The EAS-FS of both EUR and EAS groups was significantly separated, with EUR individuals closer to the EUR side and EAS individuals closer to the EAS side. (t.test $P < 2.2\times10^{-16}$, Fig. 3c).

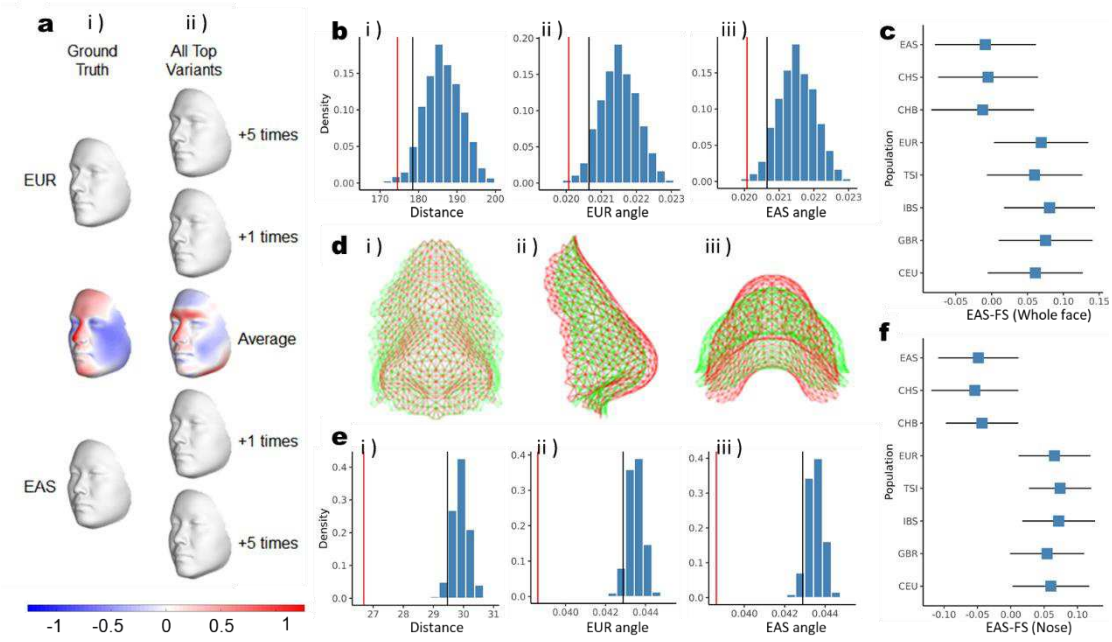

Fig. 3: Visualization of PPS derived faces of EAS and EUR and the statistical validations for PPS approach. a) Visualization of facial morphology of EAS and EUR. i) from top to bottom, representing the ground truth of EUR mean face, overall mean face (EUR and EAS), and EAS mean face respectively; ii) from top to bottom, the PPS derived faces of 244 leading variants by adding $\boldsymbol{PPS_{EUR} - PPS_{EAS}}$ +5, +1 to -1, -5 times on the overall average facial shape. Differences are visualized using the normal displacement (displacement in the direction locally perpendicular to the facial surface), blue and red refer to depression and protrusion in local shape respectively. b) The null distribution (blue) of i) Euclidean distance, ii) cosine similarity with EUR mean face, and iii) cosine similarity with EAS mean face using 1,000 simulations from 244 random variants on the whole face, red line infers the statistics of the 244 leading variants, black line infers 95% quantile of distribution from the random variants. c) The EAS-FS of polygenic shapes (whole face) for individuals in 1000GP. The squares represent the mean EAS-FS score and the horizontal lines represent 1st and 3rd quantile. d) The $\boldsymbol{PPS_{EUR} - PPS_{EAS}}$ difference of nose region in three views. i), ii), and iii) Front, side, and vertical views, respectively. The PPS derived nose of EUR and EAS are presented in the red and green color respectively. e) The distribution of i) Euclidean distance. ii) cosine similarity with EUR mean nose and iii) cosine similarity with EAS mean nose using 1,000 simulations from random variants, red line infers the statistics of the 107 leading variants associated with nose, black line infers 95% quantile of distribution from the random variants. f) The EAS-FS of polygenic shapes (nose only) for individuals in 1000GP. The squares represent the mean EAS-FS score for the nose and the horizontal lines represent 1st and 3rd quantile.

We also performed the same analyses locally in ten anatomical facial regions. The EAS and EUR derived regional facial shapes using leading variants were significantly more similar to the population mean shapes than derived shapes using random variants in the upper mouth, nose, maxillary, glabella, eye, tempora and zygoma in all three measurements of similarity, cosine similarity, Euclidean distance, and EAS-FS (seg 17,

18, 19, 24, 25, 26, 27; Extended Data Fig. 4a). Remarkably, the nasal region (seg 18) performed the best among the ten anatomical regions ($P_{EUR} = 3.7\times10^{-37}$; $P_{EAS} = 3.4\times10^{-37}$; $P_{dis} = 4.8\times10^{-33}$; Fig. 3e-f; Extended Data Fig. 4a), as shown in Fig. 3d. However, we obtained insignificant results in the mandible, forehead, and lower mouth (seg 5, 7, and 16, Extended Data Fig. 5). These results indicate that the PPS constructs morphological variations between EUR and EAS in most facial regions. In other words, the results demonstrated that the facial PPS using the leading variants identified in our study of East Asians were similar, both visually as well as statistically, to the true population mean shapes at different scales of facial shape and segments, indicating that the facial shape effects of variants in our EAS study generalize well into EUR populations.

Variants associated with East Asian facial similarity (EAS-FS)

Among the leading variants, we aimed to find those variants that make East Asians have more East Asian facial features, in other words, those variants that increase East Asian facial similarity (EAS-FS). Like the EAS-FS of an individual's PS, we first calculated the projected lengths of the variants' effect size vector onto the EAS-EUR shape difference of the whole face and the ten anatomical regions separately. We further weighted these projected lengths by their effect allele number difference of EUR and EAS as measures of each variant's contribution to EAS-EUR shape differences (Supplementary Table 5). A variant with a positive EAS-EUR shape difference may cause the EAS population's facial morphology to increase EAS facial similarity. In contrast, a variant with a negative EAS-EUR shape difference may cause the EAS population to increase EUR facial similarity. In each region (whole face and 10 anatomical regions), we constructed a distribution of the EAS-FS using 244 lead

variants. We further calculated whether each lead variant have significantly higher EAS-FS than the distribution after Bonferroni correction ($P < 0.005$) (Extended Data Fig. 6, Supplementary Fig. 3, Supplementary Table 6). As a result, 13 variants that passed filtering are regarded as increasing to EAS-FS (Table1; Supplementary Fig. 4). The 13 variants have a higher F_{ST} than the other variants (t.test $P < 1.0\times10^{-16}$)[33], indicating that these 13 variants have significant allele frequency differences between EUR and EAS. We also conducted an enrichment analysis with Population Branch Statistics (PBS), which identifies alleles that have experienced great changes in frequency in one population (EAS) relative to two reference populations (EUR and YRI)[37]. The mean PBS values of these 13 variants are significantly higher in EAS ($P < 1.0\times10^{-16}$) but not in EUR ($P = 0.188$), which suggests that these variants may be under selection in East Asian. Thus, those variants potentially have some contribution to the morphological differences between Europeans and East Asians. Most of the EAS-specific variants might be standing genetic variations as the alternative allele frequency was relatively high, given the evolutionary time, as shown in Table 1. Intriguingly, six variants had F_{ST} above 0.5 between EUR and EAS, including rs3827760 in the *EDAR* gene with the F_{ST} of 0.95, rs12632544 close to *MRPS22* with the F_{ST} of 0.60. Furthermore, three of them affected the glabella facial segment, and two of them affected the nasal region. This result also suggests that local adaption might play a role in forming facial variations between East Asians and Europeans. Among the 13 variants, six were previously reported to be associated with facial shape variation. Well-known facial genes such as *EDAR*, *TBX15* and *MRPS22* were associated with craniofacial morphology in many studies[1-4,6,9,13,15,16,38-42]. Our study shows a signal in an intron of *TBX15* (rs10923710) contributing to maxillary and tempora shape (seg 19 and 26) in EAS, consistent with the observation that this locus has multiple spatial effects on the

face[1]. The variant rs12632544 is an intergenic variant near *MRPS22* on chromosome 3q23. It was in LD (r^2 = 0.932) with rs12633011, which was reported associated with morphology of eyes in a previous East Asian study[3]. *MRPS22* has been reported to be associated with human earlobe size and a mouse skeleton phenotype[16,43,44]. A reanalysis of a GWAS study on cranioskeletal variation in outbred mice revealed that variants in the region of chromosome 9, overlapping with Mrps22, are significantly associated with craniofacial variation (FDR < 5%) (Supplementary Fig.5). The variants in this region are associated with the protrusion of the maxillary bone region, and shrinkage of the eye and malar bone region. In our study, rs12632544 contributes to EAS-FS in the glabella, eye and tempora (Extended Data Fig. 4b), which is similar to what was seen in the outbred mice. We also identified seven novel variants contributing to EAS-FS, six out of which are close to novel genes. Some of these have been reported in the context of craniofacial dysmorphology—for instance, *LHX8* and *DIS3L2*. The variant rs6669519, which contributes to the shape of glabella, is an intergenic variant near *LHX8* on chromosome 1p31.1. *LHX8*, one of the members of the LIM homeobox family of proteins, is a candidate gene for cleft palate[45]. It was also reported to be associated with forebrain neuron development and differentiation[46]. Rs12473319, associated with EAS-FS in glabella (seg 24), is an intronic variant of the DIS3 Like 3'-5' Exoribonuclease 2 (*DIS3L2*) gene (Extended Data Fig. 4c). *DIS3L2* was reported to be associated with a skeleton phenotype in a mouse genome study[44,47]. Besides, *DIS3L2* is a candidate gene for the Perlman syndrome, which is presented with craniofacial abnormalities. Moreover, the frequency of the derived C allele is higher in EAS (47.8%) than EUR (2.2%). The estimated allele age of this variant is about 7,875 years old (Table1), when the East Asians and Europeans were already two separated and diverse populations[48]. This suggests that the mutation of this variant happened in East Asians.

311 **Table 1: The 13 variants mainly associated with East Asian facial similarity (EAS-FS)**

RsID	CytoBand	A1	A2	P-value	EUR	EAS	PBS_EAS	PBS_EUR	F_{ST}_EURvEAS	Seg	Candidate gene	Allele age
rs7516137	1p36.32	C	G	9.75×10^{-29}	0.318	0.553	0.077	0.036	0.107	18	*PRDM16*	537708
rs6669519*†	1p31.1	T	A	3.40×10^{-08}	0.173	0.781	0.831	0.000	0.547	24	*LHX8*	51373
rs10923710	1p12	G	T	1.20×10^{-44}	0.193	0.507	0.262	0.000	0.207	19, 26	*TBX15*	88185
rs3827760	2q12.3	A	G	2.17×10^{-13}	0.000	0.921	2.587	0.306	0.945	27	*EDAR*	36410
rs12473319*†	2q37.1	G	C	1.35×10^{-10}	0.022	0.478	0.554	0.161	0.511	24	*DIS3L2*	39385
rs12632544	3q23	T	A	1.87×10^{-65}	0.000	0.500	0.571	0.332	0.595	24, 25, 26	*MRPS22*	626678
rs147468294	6q14.3	A	AC	9.02×10^{-17}	1.000	0.690	0.299	0.207	0.397	7	*TBX18*	46640
rs111847181	8p23.1	G	GAC	5.28×10^{-09}	0.454	0.964	0.779	0.000	0.424	18	*PPP1R3B*	788343
rs4749259*†	10p12.1	T	C	3.88×10^{-29}	0.936	0.584	0.370	0.037	0.334	26	*MKX*	298528
rs12258832*†	10p12.1	A	G	1.61×10^{-24}	0.892	0.690	0.133	0.005	0.129	26	*MKX*	64715
rs3740550*†	10q26.11	A	G	6.70×10^{-43}	0.994	0.875	0.127	0.029	0.145	19	*RAB11FIP2*	64603
rs8068343*	17q24.3	T	C	3.32×10^{-51}	0.959	0.462	0.470	0.281	0.528	18	*SOX9*	1261665
rs9980535*†	21q21.3	A	G	3.99×10^{-11}	0.176	0.762	0.357	0.380	0.521	18	*LINC00161*	1030805

312 * Novel variants in our GWAS finding, which are not in LD ($r^2 < 0.1$) with variants reported in previous facial GWAS studies, see in ST7.

313 † Novel genes in our GWAS finding, which are not reported in previous facial GWAS studies.

There are four independent association signals with nose morphology in the *SOX9* locus in our EAS GWAS (Extended Data Fig. 7) that are of interest. Although *SOX9* is a well-known gene contributing to the variation of the nose shape, rs8068343 is a novel independent variant that affects nose shape differences between populations[9,10,13]. In contrast, the other three variants may affect nose shape within populations. Compared with the previously found variants near *SOX9*, the reference (T) allele of this rs8068343 has a higher frequency in EUR (0.96) than in EAS (0.46). Moreover, this variant has a significantly higher F_{ST} (0.528) between EUR and EAS than other variants, and the iHS score of this variant is also significantly higher in CHB (2.55). These results indicate this variant may be associated with EUR-EAS nose differentiation.

Nose-associated variants show a signal of positive selection

Facial morphology exhibits a large extent of variation across human populations. In this study, East Asians show more protruded cheeks; a more concave glabella, nose, and mandible compared to Europeans. To reveal whether the variation of facial morphology in EAS and EUR populations is mainly due to natural selection or random drift, we conducted several selection analyses of the leading variants discovered here. The F_{ST} enrichment test shows that regions of the whole face and nose have a significantly higher F_{ST} than random variants after Bonferroni correction ($P_{whole\ face} = 8.22\times10^{-7}$ and $P_{nose} = 1.00\times10^{-4}$, Supplementary Table 8; Fig. 4a), indicating that facial morphology has been under natural selection between EAS and EUR, especially in the nose region[33,49]. XP-EHH enrichment analysis shows a consistent result ($P_{whole\ face} = 3.78\times10^{-3}$ and $P_{nose} = 1.27\times10^{-3}$, Supplementary Table 8; Fig. 4b) [34,35].

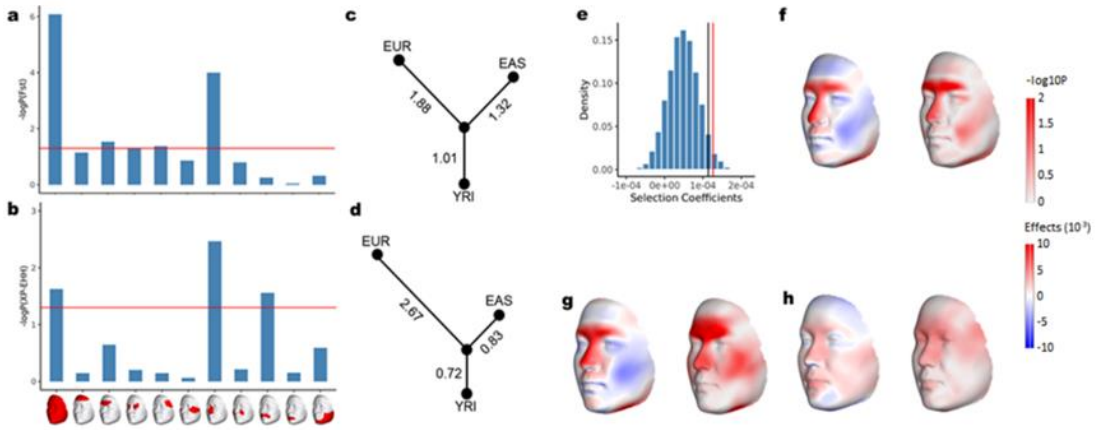

Fig. 4: Natural selection analyses and enrichment test of the differentiation of facial-associated variants among the EAS and EUR populations. a, b) P-values (-log10 scale) of a) F_{ST} and b) XP-EHH for the whole face and 10 anatomical regions. The red line is the P-value threshold of 0.05. c, d) Observed mean PBS value for the leading variants c) the 244 variants in this EAS study, and d) the 203 variants from study of White et al against the null distribution among EAS, EUR and YRI for the nose region. e) Selection coefficients for the nose region against the underlying null distribution (blue). The red line corresponds to the observed selection coefficients. The black line is 95% quantile of the null distribution. f) Differentiated accumulated genetic effects of the 244 leading variants (visualized using the local surface normal displacement) and P-values (-log10 scale) of each quasi-landmark. g) Effects and P-values (-log10 scale) of each quasi-landmark compared with random drift in the European population and in h) the East Asian population.

Next, to determine in which population the nose was primarily shaped by selection, we conducted another enrichment analysis with PBS[37]. The mean PBS values for the nose-associated loci are significantly higher than random variants in EUR ($P = 6.90\times10^{-4}$) but not in EAS ($P = 0.15$) (Supplementary Table 8, Fig. 4c), indicating that nose shape may be under subtle local selection in Europeans rather than in East Asians. In addition, we conducted the same analysis using the results of a recent published European facial GWAS[1]. Again, we found that mean PBS values for the nose-associated loci (seg 11 in

358 EUR GWAS) were significantly higher in EUR ($P_{EUR} = 9.46\times10^{-3}$) but not in EAS ($P_{EAS}$
359 = 0.464; Fig 4d). The results further prove that nose shape may be under local selection
360 in Europeans rather than East Asians.
361 The analyses above showed that the genetic variants associated with nose shape are
362 more differentiated than expected by random drift. We further analyzed the direction
363 of genetic differentiation. Based on a study of He et al, we firstly estimated and tested
364 differences using the selection coefficients for nose-increasing variants between EUR
365 and EAS[50]. In an enrichment analysis, the EUR population shows higher selection
366 coefficients for nose-increasing variants than the EAS population ($P = 4.88\times10^{-2}$)
367 (Supplementary Table 8, Fig. 4e). Moreover, by comparing the mean genetic prediction
368 of EAS and EUR's facial variation to the expected difference under random drift
369 (Methods), the nose and glabella morphology in EUR is more protruding than EAS and
370 the divergence of the nose is greater than expected under the neutral model (Fig. 4f)[32].
371 Furthermore, by comparing the PPS using the leading variants with the expected PPS
372 under random drift in the EUR and EAS population, we obtained the direction (and
373 significance) of natural selection on facial morphology in each population[32]. Similar to
374 the population differences, the nose, glabella, and zygoma are under significant natural
375 selection in the European population (Fig. 4g). However, in the East Asian population,
376 the effects of natural selection are not significant (Fig. 4h). These results suggest that
377 facial morphology in European populations undergoes local adaptation, producing a
378 more protruded nose, glabella, and flatter zygoma.
379 Based on the above results, we speculate that the differences between EAS and EUR's
380 facial features are probably due to the adaptive selection that occurred in the European
381 population, which makes Europeans have protruded and narrow noses, significantly
382 different from those of East Asians.

Discussion

In summary, as the first large-scale East Asian facial GWAS using a data-driven global-to-local phenotyping, our study greatly expanded the knowledge of craniofacial genetics outside the traditionally investigated European populations. Compared to previous facial-GWAS studies, we identified 130 (out of 244) novel variants associated with normal range facial variation, which have a similar biological function as the variants identified previously[1-18]. A considerable number of shared genetic loci were independently identified in a EUR study and this EAS study, using the same facial phenotyping approach. Among the 114 known genetic loci, 96 are associated with consistent facial regions reported in the previous facial GWAS studies. When we compare shared loci with EUR study of White et al, 82 out of 89 are associated with the same facial regions, which indicate that different segmentation patterns could attain similar GWAS results (Supplementary Table 2, Supplementary Table 4)[1]. These results suggest that the 244 genetic loci identified in our study are reliable. In addition, genetic factors associated with facial variation might be universal across populations.

We further extended the concepts of polygenic scores (PGS) to polygenic shapes (PS) to verify whether the association found in the East Asian population could be generalized to European populations[36]. Both visual insights and statistical evidence supported this hypothesis on the whole face and major anatomical facial regions. However, the PPS derived shapes of the mandible, forehead, and lower mouth are different from the corresponding European and East Asian average shapes, which is mainly due to the insufficient number of significant variants found to affect these regions. Besides the lack of phenotypic variation for East Asians in these regions, the environmental factors contributing to the facial variation may also make it harder to find enough genetic factors. In addition, the Qst, a statistic which measures phenotypic

variation contributed by genetic factors, suggested that mandible, lower mouth and forehead exhibit fewer signals of differentiation between East Asian and European populations[19]. This could explain some reason for the inconsistency of PPS for these facial regions. Of future interest is to combine all variants identified in East Asian and European studies to calculate the PPS. This might further improve the PPS in representing population averages.

Our study also provided many insights into the genetics basis of the facial shape difference between Europeans and East Asians. In addition to identifying 13 primary variants contributing to the European-Asian facial difference, we provided a method to investigate the genetic factors associated with inter-population phenotypic variations. These 13 variants all have a positive and larger than a subtle effect on the EUR-EAS facial difference, shaping the faces of East Asians to be more EAS-FS. Again, corresponding with the PPS results, due to the innate limitation of GWAS, our study overlooks rare or fixed variants in the East Asian population, which are also associated with facial variation, and which also generate more EAS-FS. If the same methods are used in a European population, additional variants affecting EAS-FS can be discovered. Moreover, for those rare or fixed variants with opposite alleles between EUR and EAS, a GWAS on a single population could never identify these, and an admixture population instead is needed.

Due to the large number of significant variants associated with the nose region, our natural selection analysis further supported the hypothesis made in the study of Zaidi et al that human nose shape has evolved in response to selection pressures[51]. Again, independent PBS studies using our signals and signals from a European study indicated that the nose shape difference between Europeans and East Asians is mainly due to natural selection in Europeans rather than in East Asians[1].

In conclusion, this study presents the largest East Asian population GWAS on 3D facial shape, using a data-driven global-to-local phenotyping. Our study revealed a large number of novel variants associated with normal range facial shape variation. In addition, by using newly introduced polygenic shapes in conjunction with validation through visualization, we successfully depicted perceptually recognizable population average faces. Such a visual feedback makes results, like ours, more tangible, comprehensive, and intuitional. Furthermore, we identified 13 variants that have large effects on East Asian facial similarity. Lastly, we provided additional good insights into the role of natural selection in shaping our face.

Reference

1. White, J.D. *et al.* Insights into the genetic architecture of the human face. *Nat Genet* **53**, 45-53 (2021).
2. Bonfante, B. *et al.* A GWAS in Latin Americans identifies novel face shape loci, implicating VPS13B and a Denisovan introgressed region in facial variation. *Sci Adv* **7**(2021).
3. Huang, Y. *et al.* A genome-wide association study of facial morphology identifies novel genetic loci in Han Chinese. *J Genet Genomics* (2020).
4. Xiong, Z. *et al.* Novel genetic loci affecting facial shape variation in humans. *Elife* **8**(2019).
5. Wu, W. *et al.* Whole-exome sequencing identified four loci influencing craniofacial morphology in northern Han Chinese. *Hum Genet* **138**, 601-611 (2019).
6. Li, Y. *et al.* EDAR, LYPLAL1, PRDM16, PAX3, DKK1, TNFSF12, CACNA2D3, and SUPT3H gene variants influence facial morphology in a Eurasian population. *Hum Genet* **138**, 681-689 (2019).
7. Qiao, L. *et al.* Genome-wide variants of Eurasian facial shape differentiation and a prospective model of DNA based face prediction. *J Genet Genomics* **45**, 419-432 (2018).
8. Crouch, D.J.M. *et al.* Genetics of the human face: Identification of large-effect single gene variants. *Proc Natl Acad Sci U S A* **115**, E676-E685 (2018).
9. Claes, P. *et al.* Genome-wide mapping of global-to-local genetic effects on human facial shape. *Nat Genet* **50**, 414-423 (2018).
10. Cha, S. *et al.* Identification of five novel genetic loci related to facial morphology by genome-wide association studies. *BMC Genomics* **19**, 481 (2018).
11. Lee, M.K. *et al.* Genome-wide association study of facial morphology reveals novel associations with FREM1 and PARK2. *PLoS One* **12**, e0176566 (2017).
12. Shaffer, J.R. *et al.* Genome-Wide Association Study Reveals Multiple Loci Influencing Normal Human Facial Morphology. *PLoS Genet* **12**, e1006149 (2016).
13. Pickrell, J.K. *et al.* Detection and interpretation of shared genetic influences on 42 human traits. *Nat Genet* **48**, 709-17 (2016).
14. Cole, J.B. *et al.* Genomewide Association Study of African Children Identifies Association of SCHIP1 and PDE8A with Facial Size and Shape. *PLoS Genet* **12**, e1006174 (2016).
15. Adhikari, K. *et al.* A genome-wide association scan implicates DCHS2, RUNX2, GLI3, PAX1 and EDAR in human facial variation. *Nat Commun* **7**, 11616 (2016).
16. Adhikari, K. *et al.* A genome-wide association study identifies multiple loci for variation in human ear morphology. *Nat Commun* **6**, 7500 (2015).
17. Paternoster, L. *et al.* Genome-wide association study of three-dimensional facial morphology identifies a variant in PAX3 associated with nasion position. *Am J Hum Genet* **90**, 478-85 (2012).
18. Liu, F. *et al.* A genome-wide association study identifies five loci influencing facial morphology in Europeans. *PLoS Genet* **8**, e1002932 (2012).
19. Guo, J. *et al.* Variation and signatures of selection on the human face. *J Hum Evol* **75**, 143-52 (2014).

20. Kanai, M., Tanaka, T. & Okada, Y. Empirical estimation of genome-wide significance thresholds based on the 1000 Genomes Project data set. *J Hum Genet* **61**, 861-866 (2016).
21. Li, J. & Ji, L. Adjusting multiple testing in multilocus analyses using the eigenvalues of a correlation matrix. *Heredity (Edinb)* **95**, 221-7 (2005).
22. Stouffer, S.A. Adjustment during army life. (1965).
23. Genomes Project, C. *et al.* A global reference for human genetic variation. *Nature* **526**, 68-74 (2015).
24. Watanabe, K., Taskesen, E., van Bochoven, A. & Posthuma, D. Functional mapping and annotation of genetic associations with FUMA. *Nat Commun* **8**, 1826 (2017).
25. McLean, C.Y. *et al.* GREAT improves functional interpretation of cis-regulatory regions. *Nat Biotechnol* **28**, 495-501 (2010).
26. Wilderman, A., VanOudenhove, J., Kron, J., Noonan, J.P. & Cotney, J. High-Resolution Epigenomic Atlas of Human Embryonic Craniofacial Development. *Cell Rep* **23**, 1581-1597 (2018).
27. Schmidt, E.M. *et al.* GREGOR: evaluating global enrichment of trait-associated variants in epigenomic features using a systematic, data-driven approach. *Bioinformatics* **31**, 2601-6 (2015).
28. Kundaje, A. *et al.* Integrative analysis of 111 reference human epigenomes. *Nature* **518**, 317-30 (2015).
29. Bernstein, B.E. *et al.* The NIH Roadmap Epigenomics Mapping Consortium. *Nat Biotechnol* **28**, 1045-8 (2010).
30. Som, P.M. & Naidich, T.P. Illustrated review of the embryology and development of the facial region, part 2: Late development of the fetal face and changes in the face from the newborn to adulthood. *AJNR Am J Neuroradiol* **35**, 10-8 (2014).
31. Zhou, Y. *et al.* Metascape provides a biologist-oriented resource for the analysis of systems-level datasets. *Nat Commun* **10**, 1523 (2019).
32. Robinson, M.R. *et al.* Population genetic differentiation of height and body mass index across Europe. *Nat Genet* **47**, 1357-62 (2015).
33. Weir, B.S. & Cockerham, C.C. Estimating F-Statistics for the Analysis of Population Structure. *Evolution* **38**, 1358-1370 (1984).
34. Gautier, M., Klassmann, A. & Vitalis, R. rehh 2.0: a reimplementation of the R package rehh to detect positive selection from haplotype structure. *Mol Ecol Resour* **17**, 78-90 (2017).
35. Sabeti, P.C. *et al.* Genome-wide detection and characterization of positive selection in human populations. *Nature* **449**, 913-8 (2007).
36. Choi, S.W., Mak, T.S. & O'Reilly, P.F. Tutorial: a guide to performing polygenic risk score analyses. *Nat Protoc* **15**, 2759-2772 (2020).
37. Yi, X. *et al.* Sequencing of 50 human exomes reveals adaptation to high altitude. *Science* **329**, 75-8 (2010).
38. Tan, J. *et al.* The adaptive variant EDARV370A is associated with straight hair in East Asians. *Hum Genet* **132**, 1187-91 (2013).
39. Kamberov, Y.G. *et al.* Modeling recent human evolution in mice by expression of a selected EDAR variant. *Cell* **152**, 691-702 (2013).
40. Ding, H.L., Clouthier, D.E. & Artinger, K.B. Redundant roles of PRDM family members in zebrafish craniofacial development. *Dev Dyn* **242**, 67-79 (2013).

41. Lausch, E. *et al.* TBX15 mutations cause craniofacial dysmorphism, hypoplasia of scapula and pelvis, and short stature in Cousin syndrome. *Am J Hum Genet* **83**, 649-55 (2008).
42. Singh, M.K. *et al.* The T-box transcription factor Tbx15 is required for skeletal development. *Mechanisms of Development* **122**, 131-144 (2005).
43. Shaffer, J.R. *et al.* Multiethnic GWAS Reveals Polygenic Architecture of Earlobe Attachment. *Am J Hum Genet* **101**, 913-924 (2017).
44. Gaudet, P., Livstone, M.S., Lewis, S.E. & Thomas, P.D. Phylogenetic-based propagation of functional annotations within the Gene Ontology consortium. *Brief Bioinform* **12**, 449-62 (2011).
45. Zhao, Y. *et al.* Isolated cleft palate in mice with a targeted mutation of the LIM homeobox gene lhx8. *Proc Natl Acad Sci U S A* **96**, 15002-6 (1999).
46. Haenig, C. *et al.* Interactome Mapping Provides a Network of Neurodegenerative Disease Proteins and Uncovers Widespread Protein Aggregation in Affected Brains. *Cell Rep* **32**, 108050 (2020).
47. Astuti, D. *et al.* Germline mutations in DIS3L2 cause the Perlman syndrome of overgrowth and Wilms tumor susceptibility. *Nat Genet* **44**, 277-84 (2012).
48. Albers, P.K. & McVean, G. Dating genomic variants and shared ancestry in population-scale sequencing data. *PLoS Biol* **18**, e3000586 (2020).
49. Guo, J. *et al.* Global genetic differentiation of complex traits shaped by natural selection in humans. *Nat Commun* **9**, 1865 (2018).
50. He, Y. *et al.* A probabilistic method for testing and estimating selection differences between populations. *Genome Res* **25**, 1903-9 (2015).
51. Zaidi, A.A. *et al.* Investigating the case of human nose shape and climate adaptation. *PLoS Genet* **13**, e1006616 (2017).

Materials and methods

Sample and recruitment details

The samples in this study were collected from three independent cohorts, the National Survey of Physical Traits (NSPT) cohort (n = 3,322), the Northern Han Chinese (NHC) cohort (n = 4,767), and the Taizhou Longitudinal Study (TZL) cohort (n = 2,881). For the NSPT sample, individuals were recruited at three Chinese cities: Nanning, Guangxi province (n = 1,326); Taizhou, Jiangsu Province (n = 986); Zhengzhou, Henan province (n = 1,010). In the Northern Han Chinese sample, participants were recruited in Tangshan, Hebei province. These two cohorts constituted the discovery dataset. The TZL cohort, where individuals were recruited in Taizhou, Jiangsu province, were used as the replication dataset. All individuals in the three cohorts were imaged using the 2-pod 3dMDface camera system.

All participants provided written informed consent, and all study protocols were approved by the institutional review boards of the pertinent research institutions. The Taizhou Longitudinal Study (TZL) was approved by the Ethics Committee of Human Genetic Resources at the Shanghai Institute of Life Sciences, Chinese Academy of Sciences (ER-SIBS-261410). The Northern Han Chinese cohort (NHC) was approved by the Ethics Committee of Human Genetic Resources at the Shanghai Institute of Life Sciences, Chinese Academy of Sciences (ER-SIBS-261410-A1801). The National Survey of Physical Traits (NSPT) is the sub project of The National Science & Technology Basic Research Project which was approved by the Ethics Committee of Human Genetic Resources of School of Life Sciences, Fudan University, Shanghai (14117).

589 **Genotyping and imputation**

590 The DNA samples of the participants in the discovery dataset were extracted from their
591 blood samples using the MagPure Blood DNA KF Kit. These DNA samples were
592 genotyped on the Illumina Infinium Global Screening Array that investigates 707,180
593 variants which is a fully custom array designed by WeGene
594 (https://www.wegene.com/). In the replication dataset, participants' DNA samples were
595 extracted from blood samples using the GENEray^{TM} DNA extraction kit. These DNA
596 samples were genotyped on the illumine HumanOmniZhongHua-8 array which
597 captures 776,213 variants. Relatedness among the individuals was inferred using
598 KING-robust separately in the discovery and replication datasets[1]. Any relative up to
599 the second-degree was excluded. As a result, 6968 (n = 4,089 in NHC cohort, n = 2,879
600 in NSPT cohort) and 2706 unrelated individuals in the discovery and replication dataset
601 are used for further analysis.

602 Since we used two different genotyping platforms in the discovery and replication
603 datasets, we chose to impute the two data sets separately. Prior to imputation, samples
604 with a genotyping missing rate > 0.05 were excluded. Haplotypes were estimated from
605 the genotypes using SHAPEIT2[2]. Then, the samples were imputed to the 1000
606 Genomes Project Phase 3 reference panel using IMPUTE2[3]. After imputation, variants
607 with an INFO score < 0.8 or certainty score < 0.9 were excluded. The discovery and
608 replication datasets were then filtered by variant missingness (--geno 0.05), minor allele
609 frequency (--maf 0.02), and Hardy Weinberg equilibrium ($P < 1\times10^{-6}$). After post-
610 imputation quality control, 8,018,212 shared variants between discovery dataset and
611 replication dataset were obtained for analysis.

612

3D image registration and quality control

After image acquisition, the 3D images were imported into MeshMonk, a 3D registration software, from wavefront.obj format files to perform a spatially dense surface registration process[4].

The nose tip landmark was manually identified as the point of origin in each 3D image to trigger an initial but crude pose alignment as input to MeshMonk. Afterwards, a symmetric anthropometric mask of 7,906 landmarks was non-rigidly mapped onto all 3D images. In each dataset (discovery and replication), generalized Procrustes analysis (GPA) was performed on a stack of the mapped 3D images and their reflection so that any difference in position, orientation, and size of both original and reflected shapes was eliminated. The average of an original and its reflected facial shape resulted in symmetrized facial shape. In this study, we were only interested in symmetrized facial shape, although the asymmetry of the human face is of great interest for future work.

After GPA and symmetrization, we investigated every mapped image manually and identified outlier images, typically exposed by locally inconsistent triangles on the surface, which are stretched and compressed irregularly in the images. Outlier images can be caused by poor quality or large noise (i.e., isolated pieces, captured position, clothes) of facial images. We removed four images with poor quality and performed the whole registration process on the noisy images again after removing the noise. In result, all 3D facial images are now represented consistently with a spatially-dense and corresponding collection of facial (quasi-)landmarks.

Facial phenotyping

Similar to the approach of Claes et al, we performed a semi-supervised facial segmentation based on the phenotypic correlation between facial landmarks using the

638 discovery dataset[5,6]. To calculate the phenotypic correlations, we first corrected the
639 symmetrized facial shapes for the covariates of age, age squared, sex, BMI, and four
640 SUGIBS components using a partial least-squares regression (PLSR, function
641 plsregress from MATLAB™ 2018a) to obtain the residual facial shapes[7]. We then
642 calculated the pairwise RV coefficients as the phenotypic 3D correlations between the
643 landmarks of the residual facial shapes. In addition to the RV similarity matrix, a scaled
644 Euclidean distances matrix (the closest points scaled to 1; the most far points scaled to
645 0) between landmarks on the anthropometric mask was calculated. This favors the
646 clustering of points closer together in 3D and therefore avoids isolated points lying
647 outside but clustered with specific facial regions, or, i.e., non-coherent facial regions.
648 Finally, we performed a hierarchical spectral clustering on a combined matrix, as
649 0.9×RV similarity matrix + 0.1×distance matrix, up to level five, resulting in a total of
650 63 facial segments (Supplementary Fig. 1).
651 In each segment, we calculate each individual's shape by adding his/her residual shape
652 from PLSR to the average shape. These shapes were aligned by a generalized Procrustes
653 analysis (GPA) followed by a principal component analysis (PCA) across the 3D
654 coordinates of the landmarks within this segment. A parallel analysis determined the
655 number of PCs retained in each segment[8]. Given the aligned shapes of a segment, we
656 performed PCA using a singular value decomposition (SVD),

657 $$\mathbf{X} \approx \mathbf{U}_{\mathrm{k}} \boldsymbol{\Sigma}_k \boldsymbol{V}_k^T \quad (1)$$

658 where $\mathbf{X}_{\mathrm{n}\times\mathrm{p}}$ is a matrix of centerized shapes with n samples and p coordinates, k
659 is the number of retained PCs, $\boldsymbol{\Sigma}_k$ is a diagonal matrix of the largest k singular values,
660 and the column vectors of $\mathbf{U}_{\mathrm{k}}$ and $\mathbf{V}_{\mathrm{k}}$ are the corresponding k left and right singular
661 vectors. In the discovery cohort, we used the left singular vectors $\mathbf{U}_{\mathrm{k}}$ as the phenotypic
662 scores of a given segment and calculated the phenotypic scores of the replication cohort,

663 $\mathbf{U}_{\mathrm{k}}^{\mathrm{r}}$, by $\mathbf{U}_{\mathrm{k}}^{\mathrm{r}} = \mathbf{X}^{\mathrm{r}}\boldsymbol{V}_k\boldsymbol{\Sigma}_k^{-1}$, where $\mathbf{X}^{\mathrm{r}}$ is the matrix of mean-centered shapes of the
664 replication cohort.
665
666 **Genome-wide association meta-analyses**
667 The meta-analysis used includes three phases, discovery, replication, and meta-analysis
668 and this following the work of White et al[6,9]. For all three phases, the genotypes were
669 coded as the number of major alleles present (0,1 or 2). In the discovery phase, in each
670 of the 63 facial segments, we used canonical correlation analysis (CCA) to define the
671 linear combination of the facial segments PCs that are mostly correlated with each
672 variant, which represent the phenotypic effect in shape space. When one of the two sets
673 of variables has only one variable, CCA reduces to multiple regression[10]. In our
674 scenario, we can calculate the CCA direction vector of a given variant by regressing
675 each shape PC onto this variant's genotypes. The resulting vector $\boldsymbol{\omega}_{\mathrm{i}}$ is also the effect
676 size vector of this variant in the shape PCA space. Besides, the correlation can be tested
677 for significance based on Rao's exact F-test (one-sided, right tail)[11]. For each variant,
678 we obtained a direction $\boldsymbol{\omega}_{\mathrm{i}}$ in the shape PCA space most correlated with the genotype
679 of that variant and a P-value representing the strength of correlation in the discovery
680 phase. In the replication phase, we calculated the Pearson's correlation between the
681 phenotypic scores and the genotypes of a given variant in the replication cohort. To test
682 the correlation's significance, we used the Student's t-test where the t-statistics is
683 defined as $t = \frac{\sqrt{\rho^2(1-\rho^2)}}{\sqrt{n-2}}$. We performed a one-sided right tail test for each variant
684 to ensure that the effective direction of the variant within the two datasets is the same.
685 Next, the P-values obtained in the discovery and replication phase were combined in a
686 meta-analysis using Stouffer's method weighted by the sample sizes[12]. We used the

corresponding implementations of these methods in the SNPLIB package to accelerate the analyses.

Conditional analysis and GWAS peak selection

For every variant, the meta-analysis described above yielded 63 P-values representing 63 facial segments. In the conditional analysis and peak selection, we selected the lowest P-value for each variant. For the initial selection, we selected the variants with P-value below the genome-wide threshold ($P = 5\times10^{-8}$) and calculated the pairwise r^2 between these variants. In each chromosome, we grouped the selected variants consecutively in a way that the r^2 between every two neighbor selected variants in the group is larger than 0.05, which resulted in 230 groups. Then for each group, we performed a conditional analysis to identify the independent signal. In detail, we first selected the variant with the lowest P-value as the conditional variant. Then, we performed association tests of the remaining variants on the condition of the conditional variant. The variant with the most significant P-value still lower than the genome-wide threshold was then added into the list of the conditional variants. We repeated these two steps until the remaining variants were not significant. Finally, we obtained 244 lead SNPs from all groups. To determine the study-wide Bonferroni P-value threshold, we calculated the number of independent tests by both the eigenvalues of the correlation matrix of the segments[13] and the permutation analysis scheme used in the study of White et al[6,14]. The numbers of independent tests obtained from the eigenvalues of the correlation matrix and the permutation analysis are 50 and 45.62, respectively. Here, we used the more stringent threshold $5\times10^{-8}/50 = 1\times10^{-9}$.

Anatomical facial regions

Following the data-driven facial segmentation, we manually selected 10 non-overlapping segments, which well fit with facial anatomy, composing the whole face. We named these segments as the following anatomical regions: forehead, glabella, eye, tempora, zygoma, nose, maxillary, upper mouth, lower mouth, and mandible. In the ten regions, forehead and mandible are located in the third layer of the 63-segmentation pattern, the remaining eight regions are located in the fifth layer. In further analysis, we accumulated the other segments variants into one of the 10 regions (Supplementary Table 3).

Gene annotation

We used three gene-mapping criteria implemented in Functional Mapping and Annotation (FUMA) to identify the candidate gene for each lead variant[15]. First, we tried to map each variant to genes based on physical distance (within a 10,000 base pair window) from the known protein-coding genes in the human reference assembly. Second, we also included the genes which have a significant eQTL association with the leading variants. We extracted the cis-eQTLs analysis, which uses a linear regression evaluated association between leading variants and expression levels of nearby genes (1 Mb distance to the leading variant), using 10 tissue types from the GTEx v8 database[16-18]. We used a false discovery rate (FDR) of 0.05 to define significant eQTL associations. Finally, we also identified candidate genes for each leading variant if there is a 3D DNA-DNA interaction between the leading variant region and the gene region, or in other words, chromatin interaction mapping. To further prioritize candidate genes, we limited interaction-mapped genes to those who interact with a predicted enhancer region identified in any of the 111 tissues or cell types from the Roadmap Epigenomics

736 Mapping Consortium (ROADMAP) and/or a gene promoter region (from 250 bp
737 upstream to 500 bp downstream of the TSS and also predicted by the ROADMAP to
738 be a promoter region)[19]. We expected that the resulting candidate genes are more likely
739 to have a plausible biological function. We used an FDR of 1×10^{-6} to define significant
740 interactions.
741 To further narrow down the candidate genes, we investigated whether any gene in the
742 window was previously associated with craniofacial development or morphology
743 through normal-range facial association studies, genetic disorders with facial
744 dysmorphology as a symptom, or animal models.
745

746 **Cell-type-specific enhancer enrichment**

747 **Chromatin state association embryonic craniofacial tissue**

748 We used GREGOR to evaluate global enrichment of trait-associated variants in
749 different chromatin states[20]. This method tests for an increase in the number of facial-
750 associated index variants, or their LD proxies ($r^2 > 0.8$), overlapping with the regulatory
751 feature more often than expected by chance by comparing to permuted control sets
752 (random control variants are selected across the genome that match the index variant
753 for a number of variants in LD, minor allele frequency and distance to nearest intron).
754 The reference epigenomes of 127 human tissues and cell types were obtained from the
755 NIH Roadmap Epigenomics Mapping Consortium[21].
756 The human embryonic craniofacial chromHMM states were obtained from each
757 Carnegie stage by Wilderman et al[22].
758

Gene expression enrichment analysis

We selected a set of transcriptome datasets from critical periods of mouse face formation that enable gene expression to be analyzed with respect to time, prominence, and tissue layer. We evaluate the expression level (fold change) of the candidate genes compare to a set of control groups where the genes were randomly selected from the genome. Then we regressed the fold change of gene expression on time, prominence, and tissue layer to test their associations.

Polygenic population shape (PPS)

Given variant i, we calculated the effect size vector $\boldsymbol{\omega}_{\mathrm{i}}$ in the shape PCA space using the discovery cohort. One can calculate the effect size vector $\boldsymbol{\beta}_{\mathrm{i}}$ in the original shape space by:

$$\boldsymbol{\beta}_{\mathrm{i}} = \mathbf{V}_{\mathrm{k}}\boldsymbol{\Sigma}_{k}\boldsymbol{\omega}_{i} \tag{2}$$

where $\boldsymbol{\Sigma}_{k}$ is a diagonal matrix of the largest k singular values and the column vectors of $\mathbf{V}_{\mathrm{k}}$ are the corresponding k right singular vectors obtained from the previous PCA (See equation (1)). Thus, the polygenic shape (PS) of an individual could be calculated as:

$$\mathbf{PS} = \sum_{\mathrm{i}}^{\mathrm{n}} \boldsymbol{\beta}_{i}\boldsymbol{g}_{i} \tag{3}$$

where $\boldsymbol{g}_{i}$ is the genotype value of variant i[23]. Subsequently, we calculate the polygenic population shape (PPS) by:

$$\mathbf{PPS} = 2\sum_{\mathrm{i}}^{\mathrm{n}} \boldsymbol{\beta}_{i}\boldsymbol{a}_{i} \tag{4}$$

where $\boldsymbol{a}_{i}$ is the effect allele frequency of variant i and two times $\boldsymbol{a}_{i}$ is the average number of effect alleles in a given population.

782

783 **East Asian and European mean facial shapes**

784 We recruited 89 individuals with self-reported European ancestry (32 females and 57
785 males) between 16 and 57 years old in Shanghai[24]. They were required to have complete
786 European ancestry over the last three generations. Their 3D facial images were captured
787 using the same protocol as used in the Chinese cohort. For the European mean facial
788 shapes, we first calculated the male and female mean facial shapes separately and used
789 the average facial shapes of these two mean shapes as the European mean facial shapes.
790 To calculate the Chinese mean facial shapes, we selected five individuals in the Chinese
791 cohort with matched age and gender to the individuals in the European cohort. We
792 finally selected 445 (5×89) individuals to calculate the Chinese mean facial shapes in
793 the same manner as in the European cohort.

794

795 **Comparison with random effects**

796 A EUR-EAS shape difference was measured to represent the degree of change in the
797 direction from the European mean face ($\bar{F}_{EUR}$) to the Chinese mean face ($\bar{F}_{EAS}$) defined
798 in the previous section. Next, we used the PPS difference between EUR and EAS
799 ($PPS_{EUR} - PPS_{EAS}$) calculated by leading variants compared with random variants to
800 evaluate whether leading variants could effectively fit the EUR-EAS shape difference.
801 We calculated the PPS derived shapes as following:

802 $$F_{EAS}^{d} = F_{AVG} - \frac{PPS_{EUR} - PPS_{EAS}}{2} \quad (5)$$

803 $$F_{EUR}^{d} = F_{AVG} + \frac{PPS_{EUR} - PPS_{EAS}}{2} \quad (6)$$

where F^d_{EAS} and F^d_{EUR} are the corresponding PPS derived shapes, F_{AVG} is the average facial shape of the population mean shapes of EUR and EAS (i.e., a population neutral average face). We performed 1000 simulations to calculate random $PPS_{EUR} - PPS_{EAS}$. In each simulation, random variants with the same effect allele frequencies in EAS were chosen to calculate random $PPS_{EUR} - PPS_{EAS}$. Subsequently, the cosine similarity and the Euclidean distances between the PPS derived shape and the corresponding mean face were used as measures of shape similarity. P-values of each approaches were then calculated using the null distribution established by these 1000 simulations.

Variants mainly associated with East-Asian face

We used the projected (vector) length to quantify a variant's contribution to the EUR-EAS face difference:

$$l_i = \frac{\mathbf{2}\left(a_i^{EUR} - a_i^{EAS}\right) \times \boldsymbol{\beta}_i \times (\overline{\boldsymbol{F}}_{EUR} - \overline{\boldsymbol{F}}_{EAS})}{|\overline{\boldsymbol{F}}_{EUR} - \overline{\boldsymbol{F}}_{EAS}|} \quad (7)$$

If a variant has a positive sign of projected length, we regard this variant to be linked to EAS individuals having more EAS features. In contrast, a variant with a negative sign is linked with EAS individuals having more EUR features.

Calculation of natural selection signatures.

We calculated genome-wide natural selection signatures based on XP-EHH using rehh2[25]. The genome-wide XP-EHH z-scores were standardized through normalization within each derived allele frequency bin (bin widths = 0.01). We estimated two-tailed P-values of the variant according to the normalized z-scores. We calculated the F_{ST} and PBS for different sets of a population[26,27]. We used the observed allele frequencies

estimated from the 1000GP Phase 3. EUR (n = 404, EUR: TSI (107), GBR (91), IBS (107), and CEU (99)), EAS (n = 208, EAS: CHB (103) and CHS (105)) and YRI (n = 103) individuals were used. Using these frequencies, we estimated pairwise F_{ST} between groups for the PBS test. The estimator is calculated as follows:

$$F_{ST} = \frac{(p_1 - p_2)^2 - \frac{p_1(1-p_1)}{n_1 - 1} - \frac{p_2(1-p_2)}{n_2 - 1}}{p_1(1-p_2) + p_2(1-p_1)} \quad (8)$$

Where for population i, n_i is the sample size and p_i is the allele frequency of the sample. F_{ST} values were transformed to calculate genetic divergence between populations as:

$$T = -\log(1 - F_{ST}) \quad (9)$$

We calculated PBS as follows:

$$PBS_X = \frac{T^{X,YRI} + T^{X,Y} - T^{YRI,Y}}{2} \quad (10)$$

Where for population X and Y, EAS and EUR were used respectively.

On the basis of a previous study, we measured selective pressures by (genic) selection coefficients[28]. For any SNP L, we can estimate the expectation of the selection (coefficient) difference per generation between populations i and j by:

$$d_{ij}(L) = \left[\ln\frac{p_i(L)}{q_i(L)} - \ln\frac{p_j(L)}{q_j(L)}\right] / t_{ij} \quad (11)$$

where p and q are the frequencies of derived and ancestral alleles in a population, respectively; and t_{ij} is the divergence time of the populations i (EUR in 1000GP) and j (EAS in 1000GP) from their most recent common ancestor. Details of the calculations are described in He et al.[28].

Phenome-wide selection signature analysis using the leading variant enrichment test.

Similar to the approach used in Guo et al[9], we compared the mean F_{ST}/PBS value of the leading variants with that of the control variants with MAF and LD score matched. First, we divided all the variants (1000GP) into 20 MAF bins from 0 to 0.5 with an increment of 0.025 (excluding the SNPs with MAF < 0.01). Each of the MAF bins was further grouped into 20 bins according to the 20 quantiles of LD score distribution. The MAF and LD score values were computed from the EAS or EUR samples in the 1000GP described above. Second, we allocated the leading variants to the MAF and LD stratified bins, randomly sampled a matched number of "control" variants from each bin, computed a mean F_{ST}/PBS value for the control variants sampled from all bins, and repeated this process 10,000 times to generate a distribution of mean F_{ST}/PBS under drift. Third, a P-value was computed from a two-tailed test by comparing the observed mean F_{ST}/PBS value for the leading variants against the null distribution quantified by the control variants, assuming normality of the null distribution. Regarding enrichment analysis of the selection signatures by XP-EHH, we obtained the sum of the squared values of the normalized XP-EHH z-scores of the variants (or the proxy variants in LD when available; $r^2 > 0.6$ in the CHB or CEU data from 1000 Genome Project), which was compared with the X^2 distribution with the degree of freedom equal to the number of the variants.

Direction of genetic differentiation.

The analysis below uses a similar method introduced in Robinson et al. to quantify the population genetic differentiation of a complex trait[29]. The leading variants' coefficients were randomized across variants 10,000 times, and 10,000 genetic predictors were

874 created in the EAS or EUR samples from the 1000GP described above. By keeping the
875 effect sizes consistent but attributing these effects across variants at random, the genetic
876 predictors generated reflect the action of genetic drift.
877

Data availability

The participants making up the NSPT, NHC and TZL datasets were not collected with broad data sharing consent. Given the highly identifiable nature of both facial and genomic information and unresolved issues regarding risk to participants, we opted for a more conservative approach to participant recruitment. Broad data sharing of the raw data from these collections would thus be in legal and ethical violation of the informed consent obtained from the participants. This restriction is not because of any personal or commercial interests. Additional details can be requested from Li Jin and Sijia Wang.

Publicly available data used were:

The 1000GP Phase 3 data:

(ftp://ftp.1000genomes.ebi.ac.uk/vol1/ftp/release/20130502/),

The Roadmap Epigenomics Project:

(https://egg2.wustl.edu/roadmap/web_portal/imputed.html#chr_imp)

The transcriptome resource from separated ectoderm and mesenchyme of the developing mouse face (GSE62214).

GWAS summary statistics are available on the National Omics Data Encyclopedia (NODE) (https://www.biosino.org/node/project/detail/OEP002283). The project ID of our study is OEP002283. Data usage shall be in full compliance with the Regulations on Management of Human Genetic Resources in China.

Code availability

KU Leuven provides the MeshMonk spatially dense facial-mapping software, free to use for academic purposes (https://github.com/TheWebMonks/meshmonk).

The statistical analyses in this work were based on MATLAB™ 2018a, SHAPEIT2 (v2.17), IMPUTE2 (v2.3.2), SNPLIB (https://github.com/jiarui-li/SNPLIB),

MeshMonk, FUMA (v1.3.6), GREAT, Metascape, REHH2 (v3.2.0), plink 1.9, R (> v.3.6), ggplot2 (v3.1.0), and Python (v3.5.0) as mentioned throughout the Methods.

Reference for Methods

1. Manichaikul, A. *et al.* Robust relationship inference in genome-wide association studies. *Bioinformatics* **26**, 2867-73 (2010).
2. Delaneau, O., Marchini, J. & Zagury, J.F. A linear complexity phasing method for thousands of genomes. *Nat Methods* **9**, 179-81 (2011).
3. Howie, B.N., Donnelly, P. & Marchini, J. A flexible and accurate genotype imputation method for the next generation of genome-wide association studies. *PLoS Genet* **5**, e1000529 (2009).
4. White, J.D. *et al.* MeshMonk: Open-source large-scale intensive 3D phenotyping. *Sci Rep* **9**, 6085 (2019).
5. Claes, P. *et al.* Genome-wide mapping of global-to-local genetic effects on human facial shape. *Nat Genet* **50**, 414-423 (2018).
6. White, J.D. *et al.* Insights into the genetic architecture of the human face. *Nat Genet* **53**, 45-53 (2021).
7. Li, J. *et al.* Robust genome-wide ancestry inference for heterogeneous datasets: illustrated using the 1,000 genome project with 3D facial images. *Sci Rep* **10**, 11850 (2020).
8. Horn, J.L. A Rationale and Test for the Number of Factors in Factor Analysis. *Psychometrika* **30**, 179-85 (1965).
9. Guo, J. *et al.* Global genetic differentiation of complex traits shaped by natural selection in humans. *Nat Commun* **9**, 1865 (2018).
10. Willer, C.J., Li, Y. & Abecasis, G.R. METAL: fast and efficient meta-analysis of genomewide association scans. *Bioinformatics* **26**, 2190-1 (2010).
11. Olson & Chester, L. On choosing a test statistic in multivariate analysis of variance. *Psychological Bulletin* **83**, 579-586 (1976).
12. Stouffer, S.A. Adjustment during army life. (1965).
13. Li, J. & Ji, L. Adjusting multiple testing in multilocus analyses using the eigenvalues of a correlation matrix. *Heredity (Edinb)* **95**, 221-7 (2005).
14. Kanai, M., Tanaka, T. & Okada, Y. Empirical estimation of genome-wide significance thresholds based on the 1000 Genomes Project data set. *J Hum Genet* **61**, 861-866 (2016).
15. Watanabe, K., Taskesen, E., van Bochoven, A. & Posthuma, D. Functional mapping and annotation of genetic associations with FUMA. *Nat Commun* **8**, 1826 (2017).
16. Carithers, L.J. & Moore, H.M. The Genotype-Tissue Expression (GTEx) Project. *Biopreserv Biobank* **13**, 307-8 (2015).
17. Keen, J.C. & Moore, H.M. The Genotype-Tissue Expression (GTEx) Project: Linking Clinical Data with Molecular Analysis to Advance Personalized Medicine. *J Pers Med* **5**, 22-9 (2015).
18. Lonsdale, J. *et al*. The Genotype-Tissue Expression (GTEx) project. *Nat Genet* **45**, 580-5 (2013).
19. Kundaje, A. *et al.* Integrative analysis of 111 reference human epigenomes. *Nature* **518**, 317-30 (2015).
20. Schmidt, E.M. *et al.* GREGOR: evaluating global enrichment of trait-associated variants in epigenomic features using a systematic, data-driven approach. *Bioinformatics* **31**, 2601-6 (2015).
21. Bernstein, B.E. *et al.* The NIH Roadmap Epigenomics Mapping Consortium. *Nat Biotechnol* **28**, 1045-8 (2010).

22. Wilderman, A., VanOudenhove, J., Kron, J., Noonan, J.P. & Cotney, J. High-Resolution Epigenomic Atlas of Human Embryonic Craniofacial Development. *Cell Rep* **23**, 1581-1597 (2018).
23. Choi, S.W., Mak, T.S. & O'Reilly, P.F. Tutorial: a guide to performing polygenic risk score analyses. *Nat Protoc* **15**, 2759-2772 (2020).
24. Guo, J. *et al.* Variation and signatures of selection on the human face. *Journal of Human Evolution* **75**, 143-152 (2014).
25. Gautier, M., Klassmann, A. & Vitalis, R. rehh 2.0: a reimplementation of the R package rehh to detect positive selection from haplotype structure. *Mol Ecol Resour* **17**, 78-90 (2017).
26. Weir, B.S. & Cockerham, C.C. Estimating F-Statistics for the Analysis of Population Structure. *Evolution* **38**, 1358-1370 (1984).
27. Yi, X. *et al.* Sequencing of 50 human exomes reveals adaptation to high altitude. *Science* **329**, 75-8 (2010).
28. He, Y. *et al.* A probabilistic method for testing and estimating selection differences between populations. *Genome Res* **25**, 1903-9 (2015).
29. Robinson, M.R. *et al.* Population genetic differentiation of height and body mass index across Europe. *Nat Genet* **47**, 1357-62 (2015).

Acknowledgements

This project was funded by the following grants and contracts: Shanghai Municipal Science and Technology Major Project (2017SHZDZX01, 2018SHZDZX01); National Key Research and Development Project 2018YFC0910403; CAS Interdisciplinary Innovation Team Project; "Strategic Priority Research Program" of the Chinese Academy of Sciences (Grant No. XDB38020400); Max Planck-CAS Paul Gerson Unna Independent Research Group Leadership Award; National Natural Science Foundation of China (Grant No.31521003, Grant No.31900408); National Science & Technology Basic Research Project 2015FY111700; CAMS Innovation Fund for Medical Sciences 2019-I2M-5-066; The 111 Project B13016; China Postdoctoral Science Foundation (No.2019M651352, No. 2020M670984).

We thank for all suggestions collected during the poster exhibition of ASHG 2019 Annual Meeting. We thank all the participants in these studies.

Author contributions

S.Wang., L.J., J.L., and M.Z. conceptualized the study (ideas; formulation or evolution of overarching research goals and aims). M.Z, S.Wu., S.D., W.Q. and J.L. carried out the data curation (management activities to annotate, scrub data and maintain research data for initial use and later re-use). M.Z, S.Wu., S.D., W.Q., J.L. and J.C. carried out the formal analysis (application of statistical, mathematical, computational, or other formal techniques to analyze or synthesize study data). M.Z, S.Wu., S.D., W.Q. and J.L. did the visualization (preparation, creation and/or presentation of the published work, specifically visualization/data presentation). K.T. and L.Q., Y.Y. and J.T. collected the 3D facial scans of the TZL cohort. J.T, K.T. and L.Q. collected the 3D facial scans of the NSPT cohort. S.Wu., S.D., and J.L. registered the 3D facial scans of the Northern

Han Chinese cohort and conducted the PCA of discovery cohort. N.N. and A.R.L. performed the analysis of *MPRS22*/Mprs22 and human/mouse craniofacial shape. M.Z, S.Wu., S.D., W.Q. and J.L. wrote the original draft. S.Wang., L.J., P.C., J.L., M.Z, S.Wu., S.D., and W.Q. reviewed and edited the final manuscript. All authors participated in preparing the manuscript by reading and commenting on drafts before submission.

Competing interest declaration

The authors declare no competing interests.

Corresponding author

Correspondence to Sijia Wang, Jiarui Li or Li Jin.

Sijia Wang, wangsijia@picb.ac.cn

Jiarui Li, lijiarui@picb.ac.cn

Li Jin, lijin@fudan.edu.cn

Additional Information

Extended Data Figures

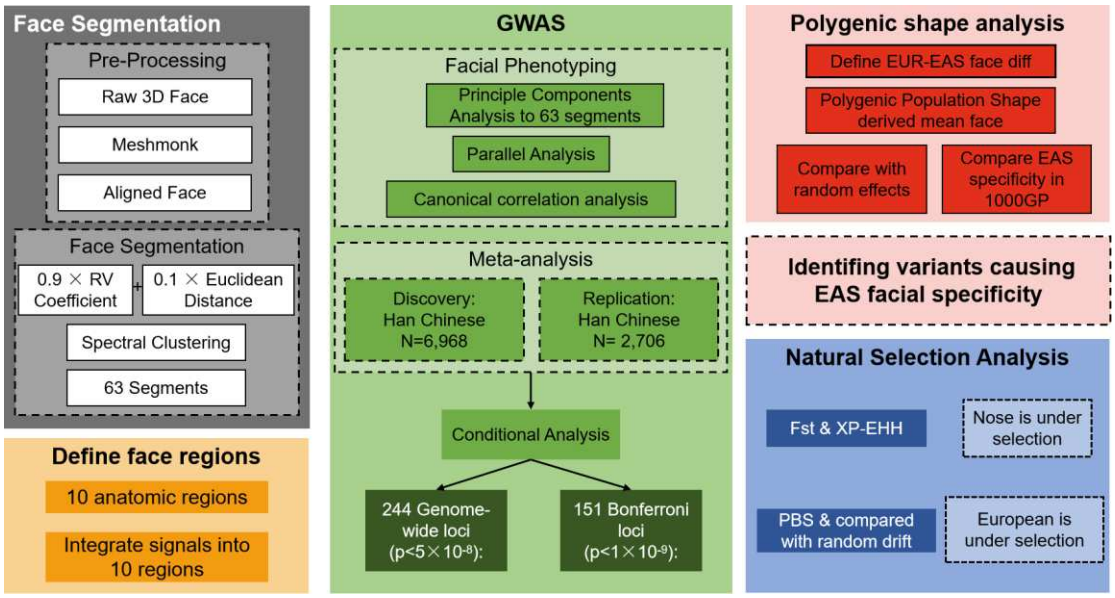

Extended Data Fig. 1: Study design.

We first start with a face segmentation procedure to get 63 face segments from which we defined 10 anatomical face regions. Then by using a CCA based GWAS, we identified 244 variants with a P-value lower than 5×10^{-8}, in which 151 are also lower than 1×10^{-9}. To investigate what affects the similarity of an EAS face, we used polygenic population shape (PPS) analyses to fit EUR and EAS faces and identified 13 variants mainly contributing to EUR-EAS facial differences. To investigate selection on facial variation, we used F_{ST} and XP-EHH to find which parts of the face are under selection. These results, we further compared with random drift and random PPS to find out, which from the two populations, EUR or EAS, experienced selection.

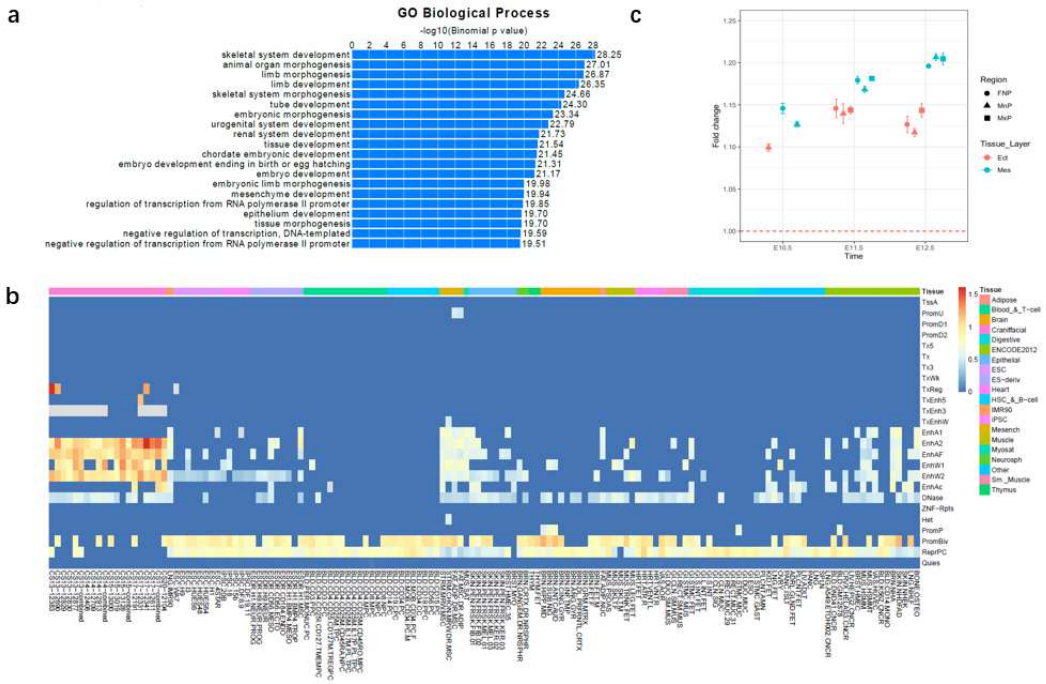

Extended Data Fig. 2: Enrichment analysis of leading variants.

(a) Geno Ontology enrichment for genes annotated from leading variants by GREAT.

(b) Heatmap indicating the global enrichment of trait-associated variants in different chromatin state (y axis) and in different tissue (x axis). The fold change was calculated by GREGOR. The embryonic craniofacial tissue was previously published by epigenomic atlas, while the other was previously published by Roadmap Epigenome. The description of the 25-state chromatin model can be found at: https://egg2.wustl.edu/roadmap/web_portal/imputed.html#chr_imp.

(c) Expression levels of the candidate genes in craniofacial tissues. Each point represents an estimated fold change compared to control genes at different times (E10.5, E11.5, E12.5), in different prominences (Frontonasal, FNP: circle; Maxillary, MxP: square; Mandibular, MnP: triangle), and tissue layer (Ectoderm, Ect: red; Mesenchyme, Mes: blue) with 95% confidence intervals.

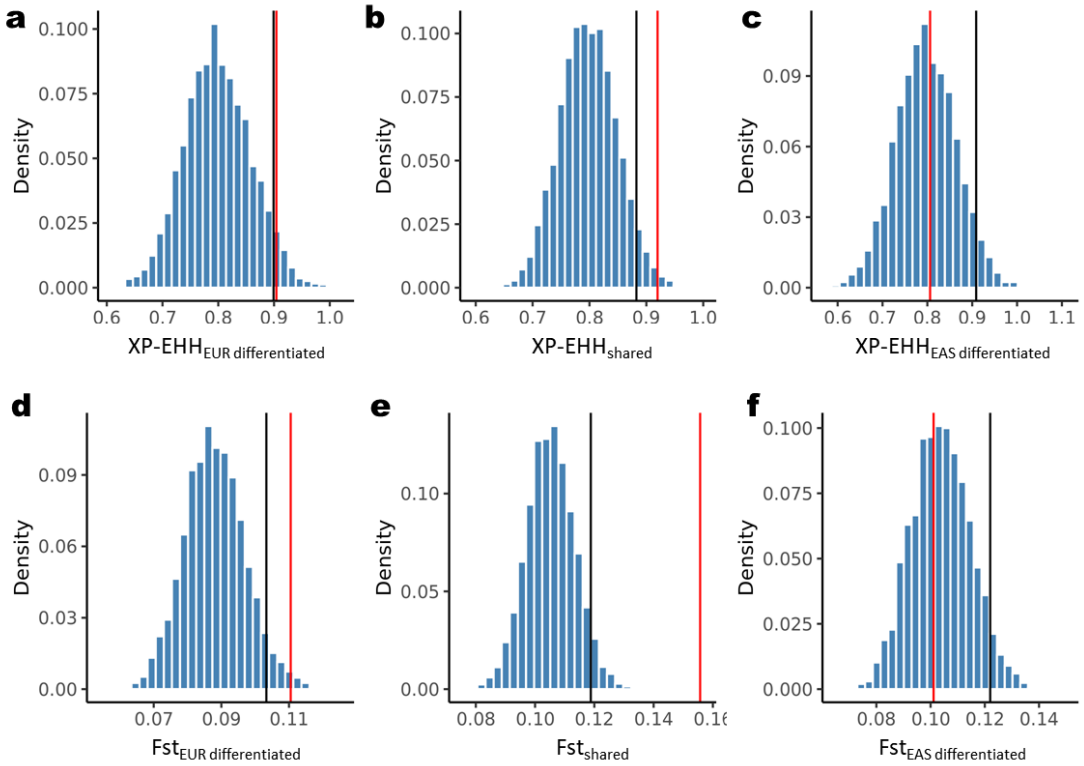

Extended Data Fig. 3: XP-EHH and F_{ST} enrichment analysis for shared and differentiated variants

XP-EHH and F_{ST} enrichment analysis for (a, d) EUR differentiated variants, (b, e) EAS differentiated variants, and (c, f) shared variants in EAS study. The blue color is the null distribution. The red line is the mean XP-EHH or F_{ST} score of shared or differentiated variants. The black line is the 95% quantile of the null distribution.

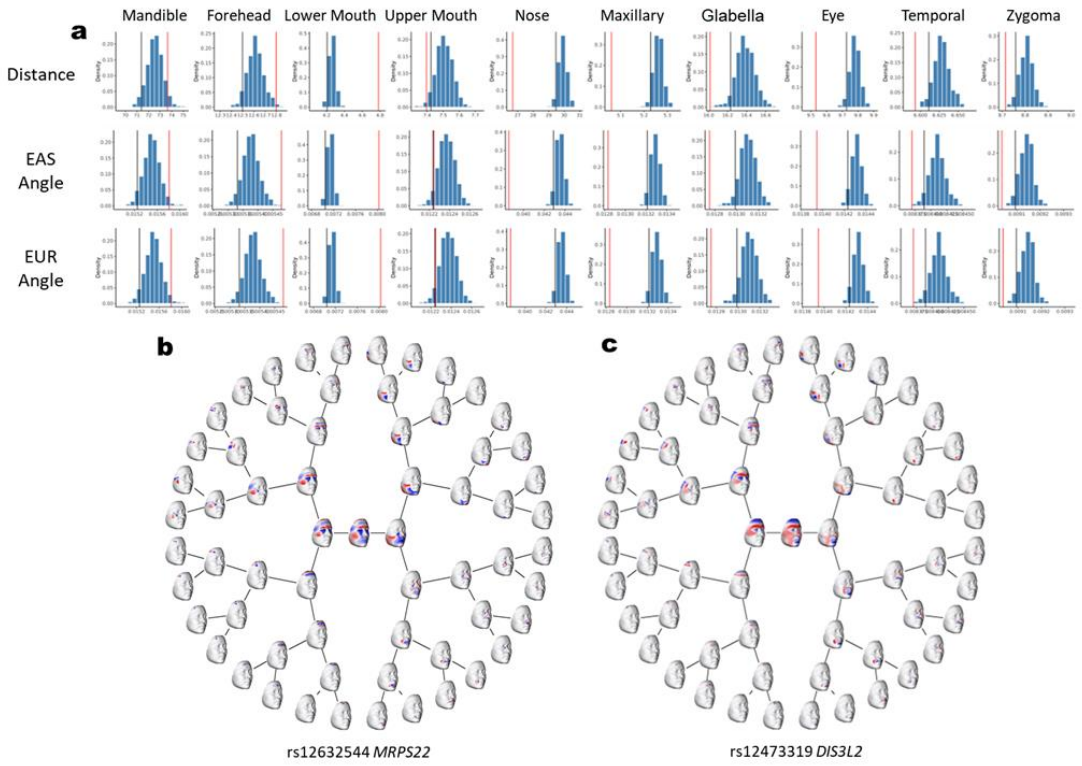

1053

1054 **Extended Data Fig. 4: Validation of PPS in 10 anatomical segments.**

1055 a) The null distribution (blue) of Euclidean distance, cosine similarity with EUR mean face and
1056 EAS mean face using 1,000 simulations derived from random variants on the 10 anatomical
1057 regions, red line infers the statistics of the leading variants associated with corresponding
1058 regions; black line infers 95% quantile of distribution from the random variants with
1059 corresponding regions; b) The genetic effects of rs12632544 and c) rs12473319 weighted by
1060 their effect allele number difference of EUR and EAS (visualized using the local surface normal
1061 displacement) .

1062

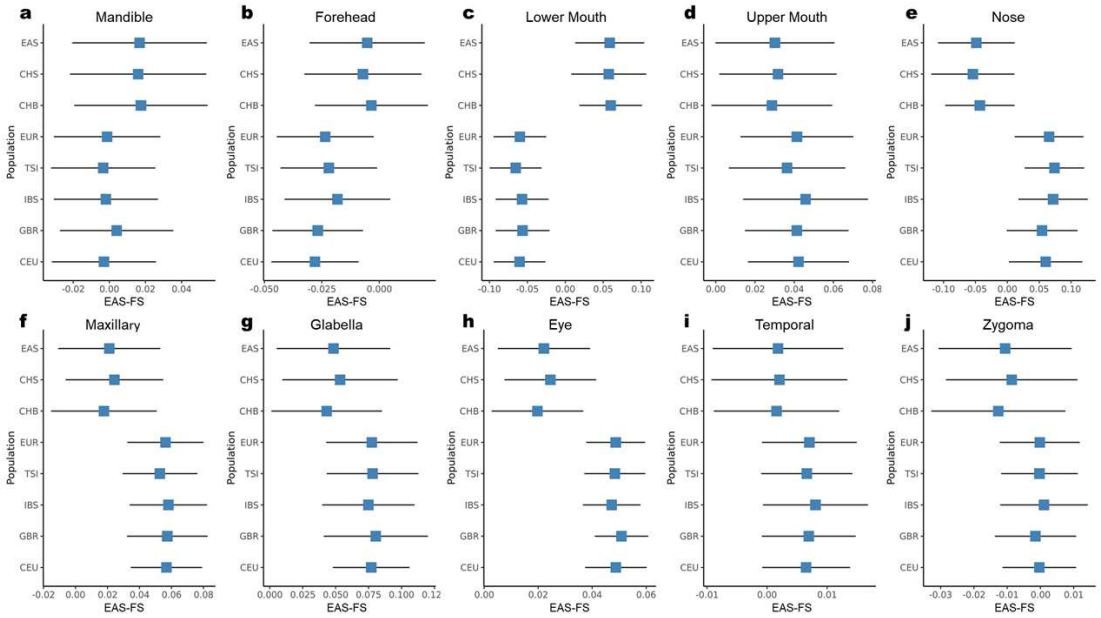

1063

1064 **Extended Data Fig. 5: The EAS-FS of polygenic shapes in 10 anatomical regions for EAS**
1065 **and EUR individuals in 1000GP.**

1066 The EAS-FS of polygenic shapes in a) mandible, b) forehead, c) lower mouth, d) upper mouth,
1067 e) nose, f) maxillary, g) glabella, h) eye, i) tempora, and j) zygoma for EAS and EUR
1068 individuals in 1000GP. The squares represent the mean EAS-FS score in 10 anatomical regions
1069 and the horizontal lines represent 1st and 3rd quantile.

1070

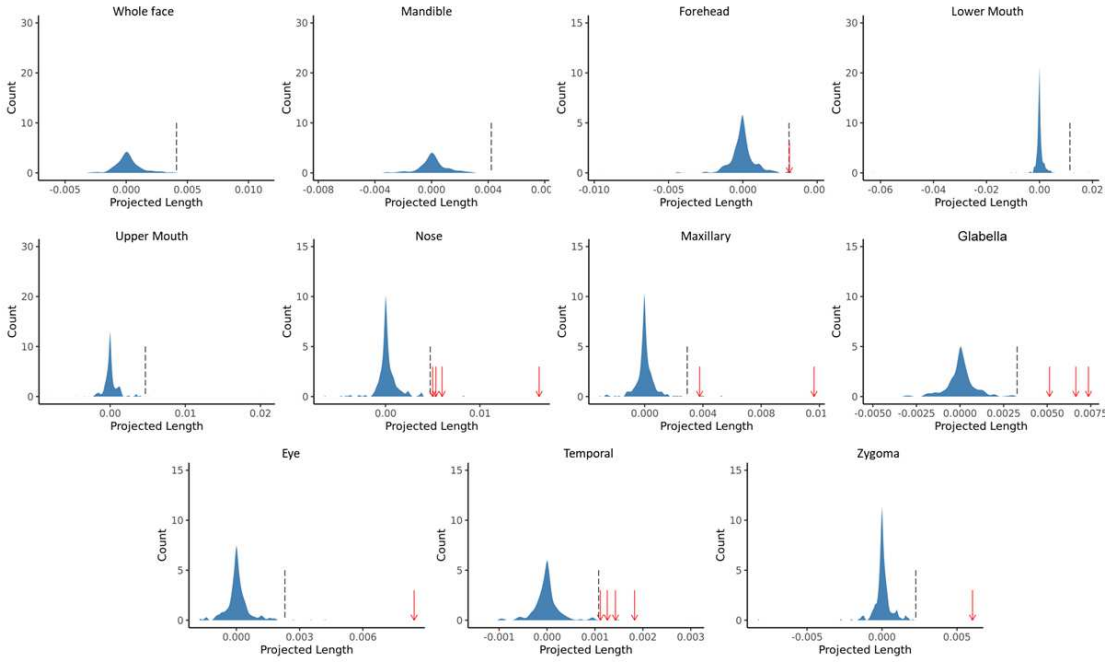

1071

1072 **Extended Data Fig. 6: EAS-FS of the 244 leading variants on the EUR-EAS difference.**

1073 The distributions (blue) of EAS-FS derived from 244 leading variants associated with a) whole
1074 face and b) - k) 10 anatomical segments. The black dotted line is the EAS-FS threshold of each
1075 region (mean + 3×SD). The red arrow is the variant over threshold.

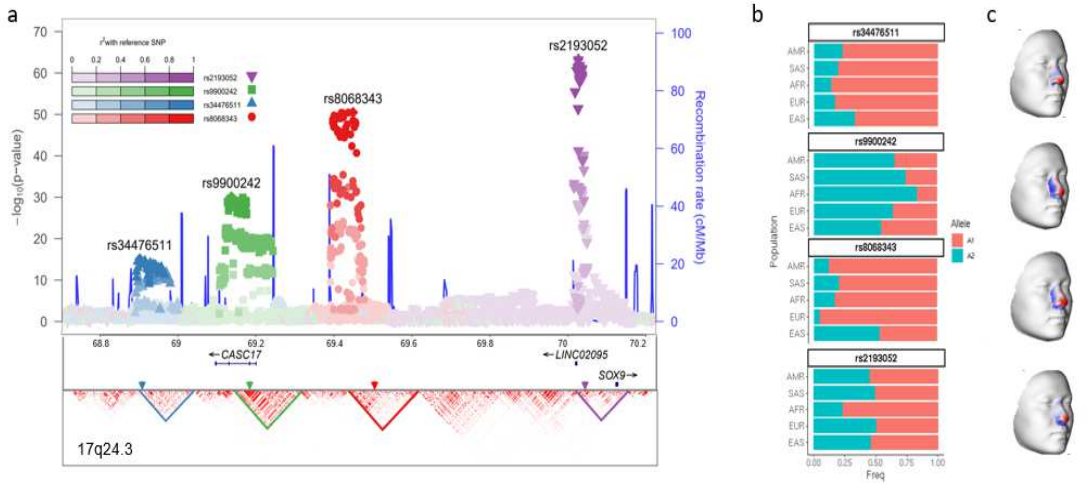

Extended Data Fig. 7: Multi peak in 17q24.3 region.

a) Association signals in the SOX9 locus and genomic environment surrounding SOX9 across a 2-Mb window. Four independent signals, represented by (1) rs34476511 (blue), (2) rs9900242 (green), (3) rs8068343 (red), and (4) rs2193052 (purple) are observed; b) Allele frequency in AMR, SAS, AFR, EUR and EAS population of the four variants from 1000GP; c) The effects of the four variants in the nose region.

Supplementary Files

Supplementary Tables:

Supplementary Table 1. Characteristic of all cohorts.

Supplementary Table 2. 244 lead variants associated with normal-range variation.

Supplementary Table 3. The associated anatomical regions (and segments) of each lead variant.

Supplementary Table 4. The shared and differentiated variants of EAS and EUR study.

Supplementary Table 5. The East-Asian facial similarity (EAS-FS) of 244 lead variants in whole face and 10 anatomical regions.

Supplementary Table 6. The Standard deviation (SD) of East Asian facial similarity (EAS-FS) of 244 lead variants in whole face and 10 anatomical regions.

Supplementary Table 7. A list of facial associated candidate gene variants previously reported in facial GWASs.

Supplementary Table 8. P-value of natural selection enrichment analyses for 11 facial regions.

Supplementary Figures

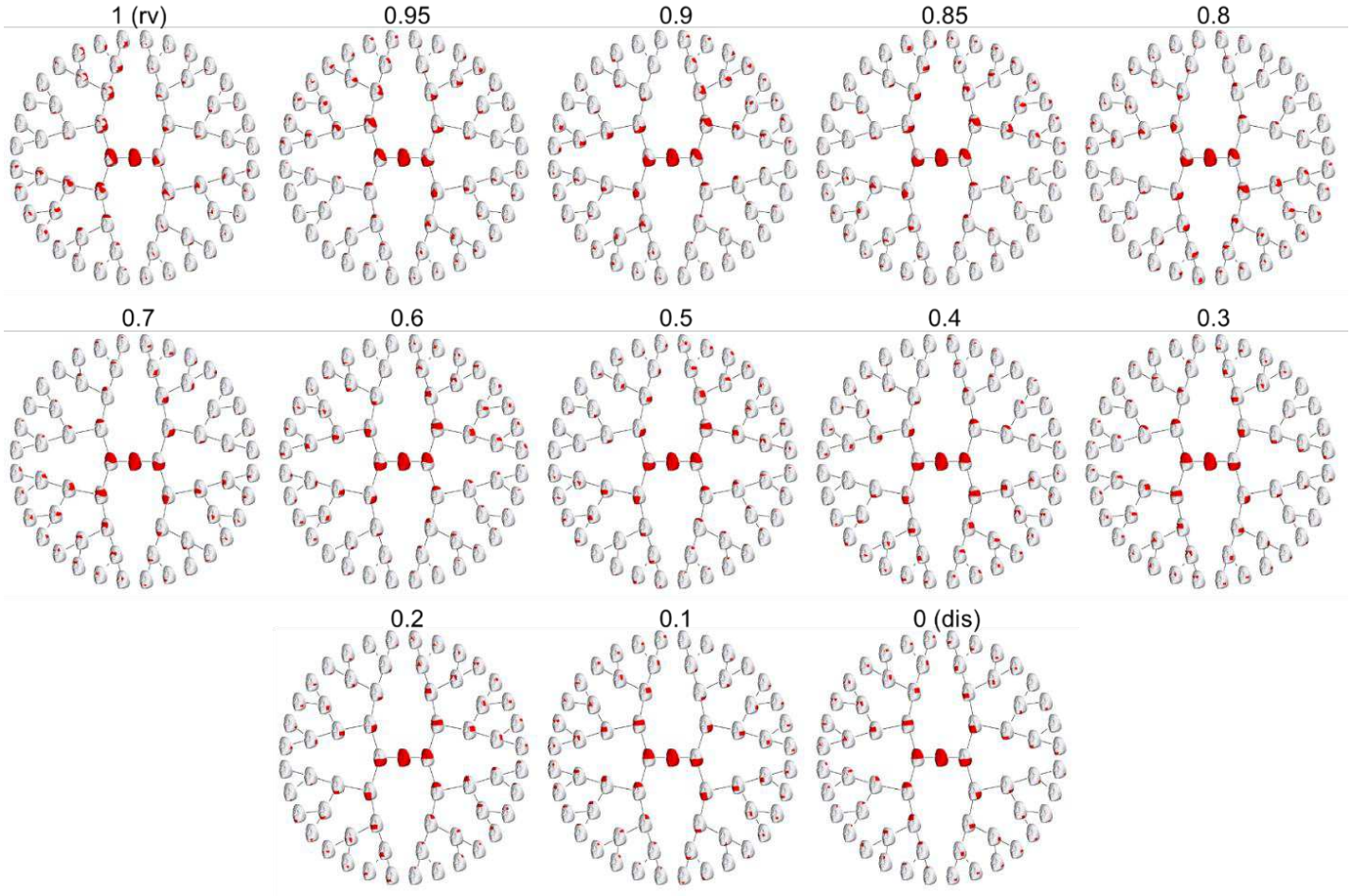

Supplementary Figure 1: Segmentation pattern of a series of RV and distance matrix combination.

Using the only RV matrix (the first pattern), we found that there are many isolated points or discrete pieces. This kind of segmentation pattern are hard to make further biological interpretation. To obtain continuous segmentation pattern, we used pair-wised distance matrix as the regularization parameter. We aimed to obtain a continuous segmentation pattern without isolated points or discrete pieces, meanwhile keep the weight of RV matrix as great as possible. Following this criteria, we found when 0.9 RV matrix and 0.1 distance matrix are combined, there are no isolated points or discrete pieces, thus the segmentation pattern are continuous. Moreover, we found this segmentation pattern are corresponding with anatomical regions, which makes it easier to make further biological interpretations. The red square is the final used segmentation pattern.

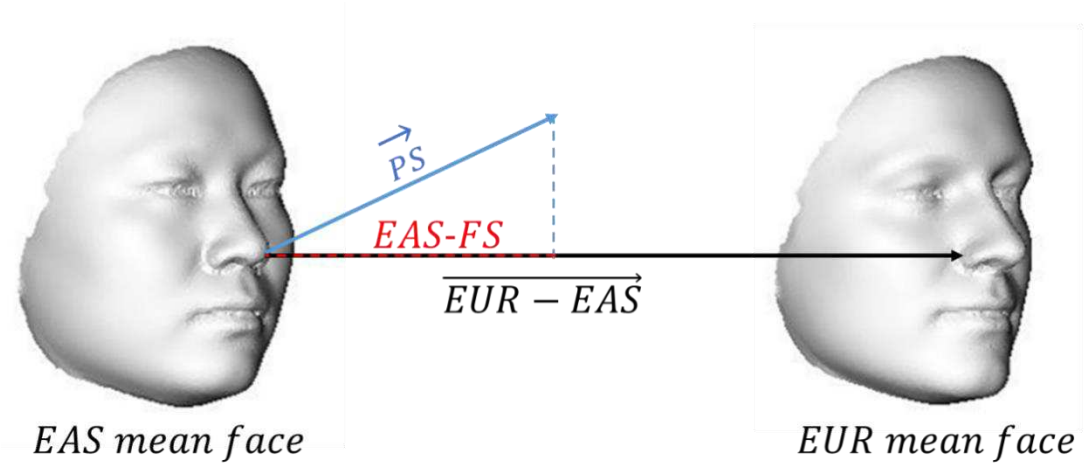

Supplementary Figure 2: The schematic diagram of calculating the EAS-FS in 1000GP individuals

The schematic diagram of calculating the EAS facial similarity (EAS-FS) for each individuals. The black arrow is the vector of differences in facial shape from EAS to EUR. The blue arrow is the vector of PS. The EAS-FS value of each individual is obtained by projecting vector PS to vector EUR-EAS.

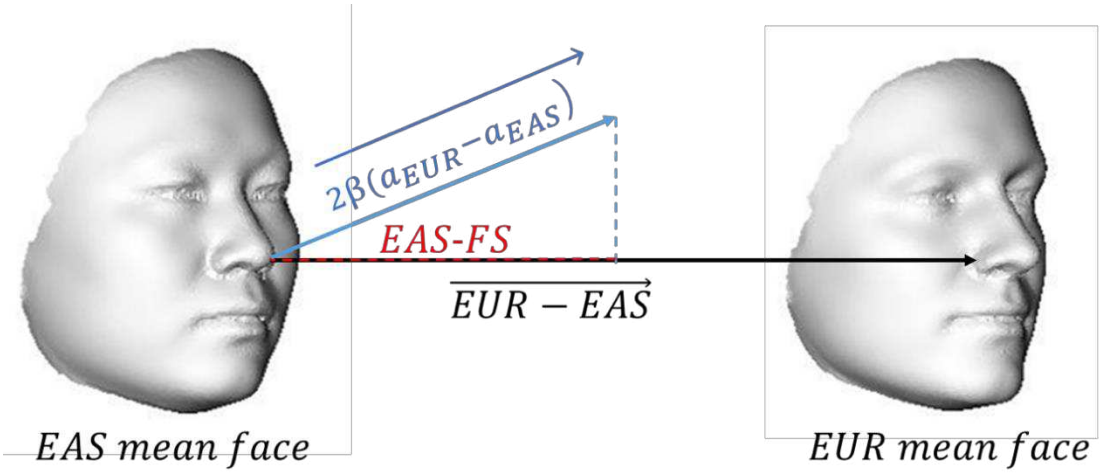

Supplementary Figure 3: The schematic diagram of calculating each variant's EAS-FS.

The schematic diagram of calculating the EAS facial similarity (EAS-FS) of each lead variant. The black arrow is the vector of differences in facial shape from EAS to EUR. The Blue arrow is the vector of effects of each variants weight by the effect allele number difference of EUR and EAS. The EAS-FS value of each variant is obtained by projecting vector weighed effects of each variant to vector EUR-EAS.

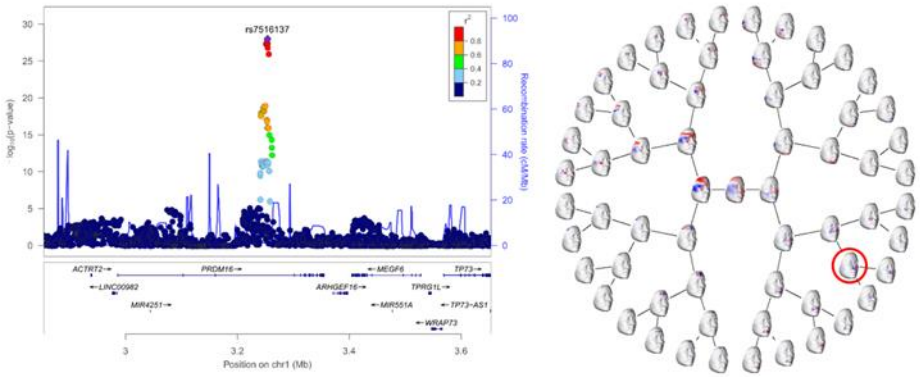
rs7516137
ACTRT2→
PRDM16→
←MEGF6
TP73→
←LINC00982
ARHGEF16→
TPRG1L→
MIR4251→
←MIR551A
←TP73-AS1
←WRAP73
Position on chr1 (Mb)
Recombination rate (cM/Mb)

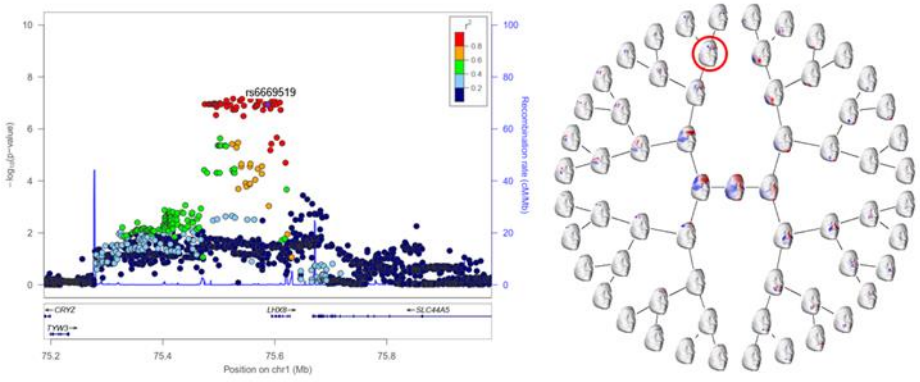
rs6669519
←CRY2
LHX9→
←SLC44A5
TYW1→
Position on chr1 (Mb)
Recombination rate (cM/Mb)

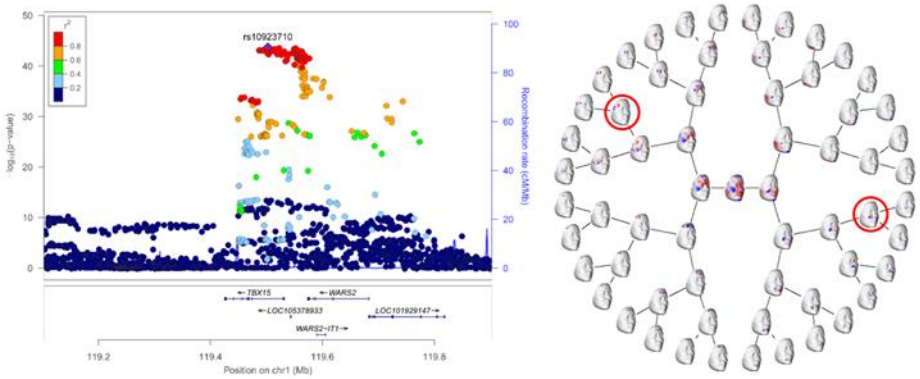
rs10923710
←TBX15
←WARS2
←LOC105378933
LOC101929147→
WARS2-IT1→
Position on chr1 (Mb)
Recombination rate (cM/Mb)

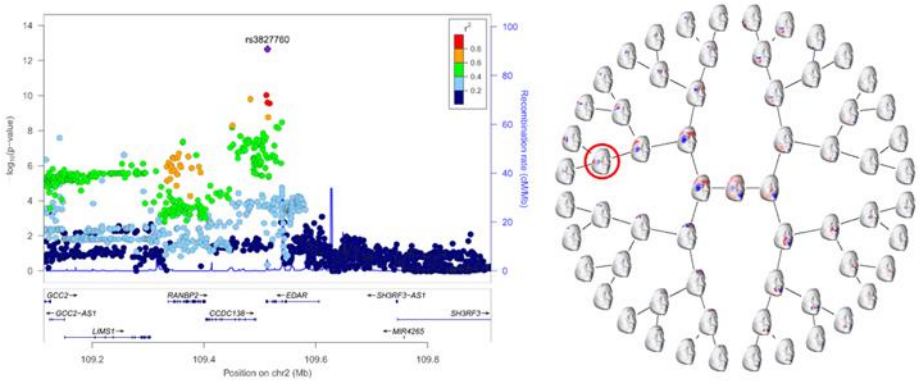
rs3827760
GCC2→
RANBP2→
←EDAR
←SH3RF3-AS1
←GCC2-AS1
CCDC138→
SH3RF3→
LIMS1→
←MIR4265
Position on chr2 (Mb)
Recombination rate (cM/Mb)

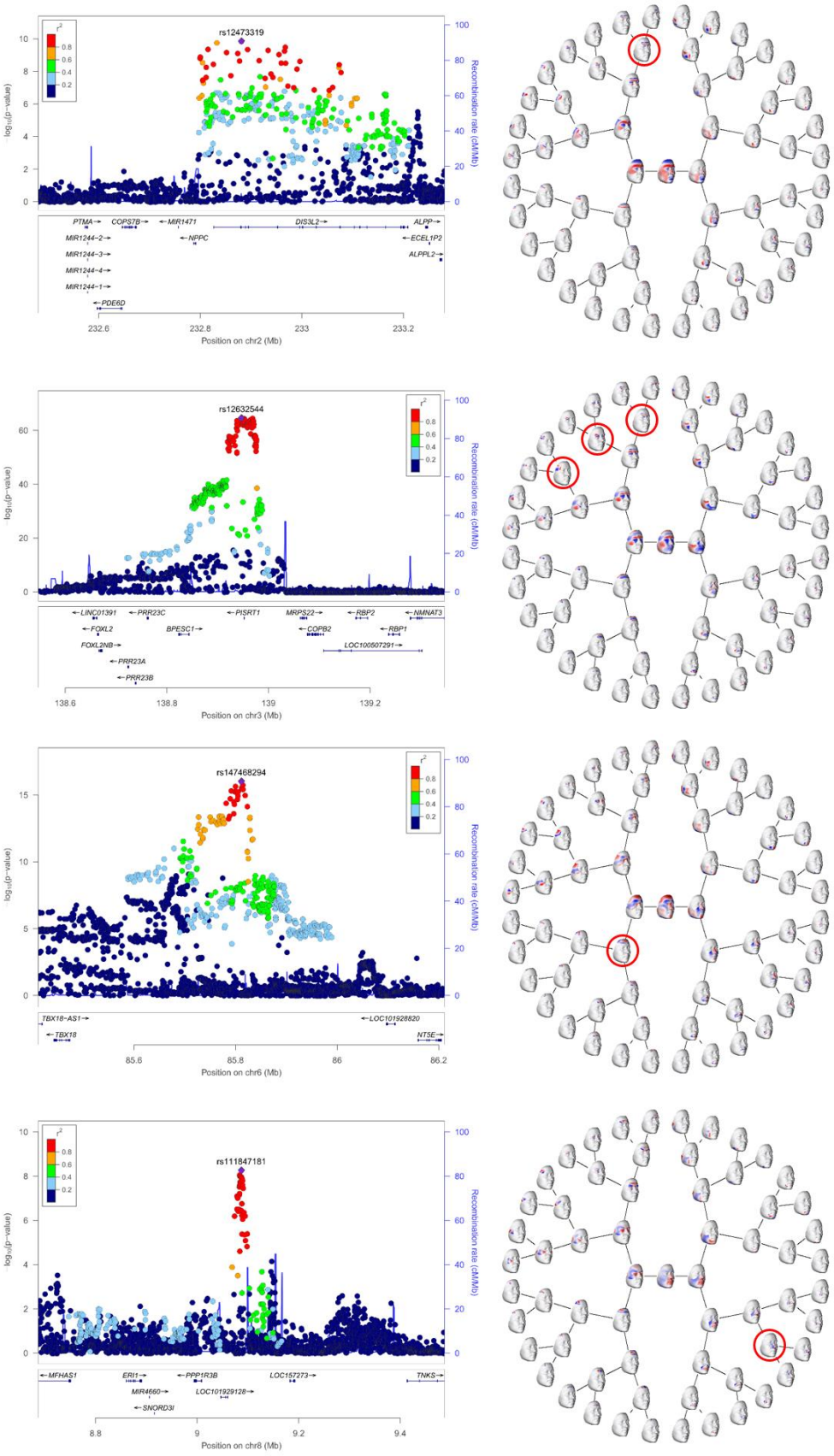
rs12473319
PTMA
COPS7B
MIR1471
DIS3L2
ALPP
MIR1244-2
NPPC
ECEL1P2
MIR1244-3
ALPPL2
MIR1244-4
MIR1244-1
PDE6D
232.6
232.8
233
233.2
Position on chr2 (Mb)
rs12632544
LINC01391
PRR23C
PISRT1
MRPS22
RBP2
NMNAT3
FOXL2
BPESC1
COPB2
RBP1
FOXL2NB
LOC100507291
PRR23A
PRR23B
138.6
138.8
139
139.2
Position on chr3 (Mb)
rs147468294
TBX18-AS1
LOC101928820
TBX18
NT5E
85.6
85.8
86
86.2
Position on chr6 (Mb)
rs111847181
MFHAS1
ERI1
PPP1R3B
LOC157273
TNKS
MIR4660
LOC101929128
SNORD3I
8.8
9
9.2
9.4
Position on chr8 (Mb)
Recombination rate (cM/Mb)

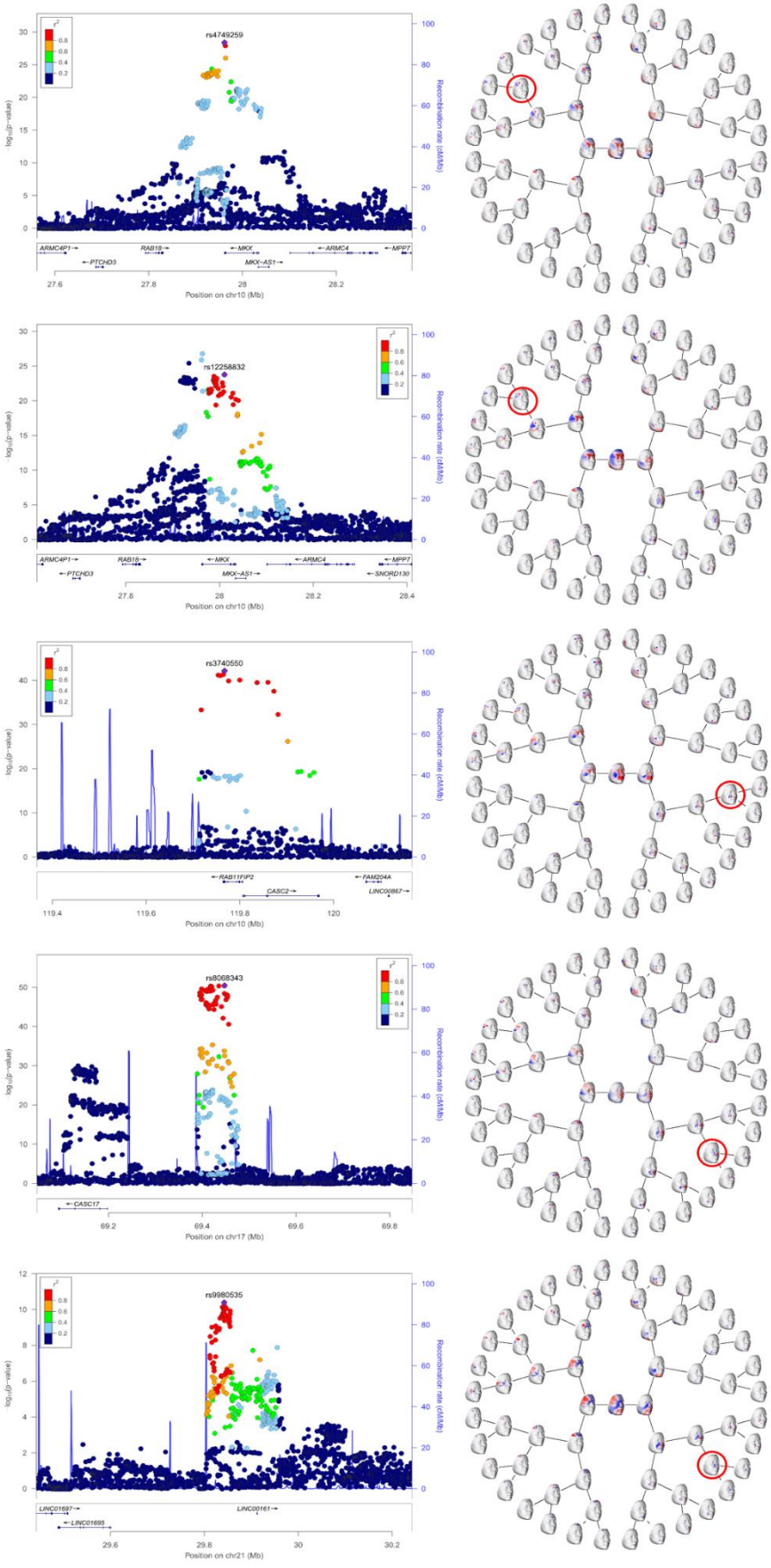
rs4749259
ARMC4P1→
RAB18→
←MKX
←ARMC4
←MPP7
←PTCHD3
MKX-AS1→
Position on chr10 (Mb)
rs12258832
←SNORD130
Position on chr10 (Mb)
rs3740550
←RAB11FIP2
←FAM204A
GASC2→
LINC00867→
Position on chr10 (Mb)
rs8068343
←CASC17
Position on chr17 (Mb)
rs9980535
LINC01697→
LINC00161→
←LINC01695
Position on chr21 (Mb)

Supplementary Figure 4: Effects of 13 variants associated with EAS-FS.

On the left are the Locuszoom of 13 variants associated with EAS-FS. On the right are the genetic effects of 13 variants weighted by the effect allele number difference of EUR and EAS. The red circle are the facial region(s) that the variant associated with EAS-FS.

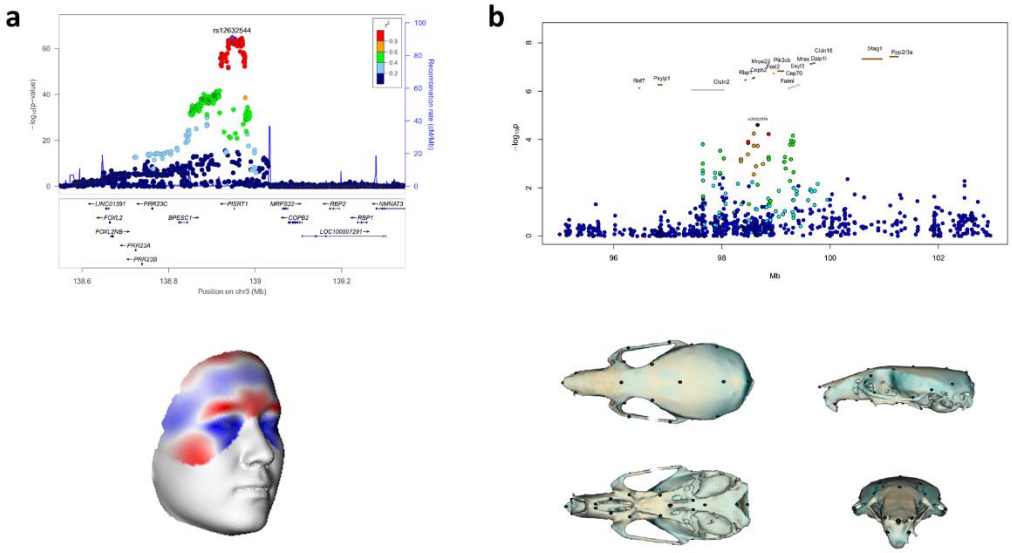

Supplementary Figure 5: ***MPRS22*****/Mprs22 and human/mouse craniofacial shape**.

a) Regional association P-values (index SNP is labeled) are shown at the left top. The genetic effects on the human whole face of rs12632544 weighted by the effect allele number difference of EUR and EAS (visualized using the local surface normal displacement) are shown at the left bottom.

b) Regional association plot for the Mprs22 homologous region in chromosome 9 among outbred mice. Phenotypic effect associated with allele dosage at the Mprs22 index SNP among outbred mice. Skull zones with an expansion/contraction relative to the mean shape are shown in brown/blue.

Supplementary Files

This is a list of supplementary files associated with this preprint. Click to download.

- 3DAlltables.xlsx
- nrreportingsummary3Dpaper0615.pdf